

Exploring Roles of MiR-372-3p in Proliferation of Hepatocellular Carcinoma Cells



Mr. Pannathon Thamjamrassri

A Thesis Submitted in Partial Fulfillment of the Requirements
for the Degree of Master of Science in Medical Biochemistry

Department of Biochemistry

FACULTY OF MEDICINE

Chulalongkorn University

Academic Year 2022

Copyright of Chulalongkorn University



จุฬาลงกรณ์มหาวิทยาลัย
CHULALONGKORN UNIVERSITY

การศึกษบทบาทในการเพิ่มจำนวนเซลล์มะเร็งระดับของไมโครอาร์เอ็นเอสามเจ็ดสองสามพี



วิทยานิพนธ์นี้เป็นส่วนหนึ่งของการศึกษาตามหลักสูตรปริญญาวิทยาศาสตรมหาบัณฑิต
สาขาวิชาชีวเคมีทางการแพทย์ ภาควิชาชีวเคมี
คณะแพทยศาสตร์ จุฬาลงกรณ์มหาวิทยาลัย
ปีการศึกษา 2565
ลิขสิทธิ์ของจุฬาลงกรณ์มหาวิทยาลัย

ปณิธาน ธรรมจรรย์สรี : การศึกษาบทบาทในการเพิ่มจำนวนเซลล์มะเร็งระดับของไมโครอาร์เอ็นเอสาม
 เจ็ดสองสามพี. (Exploring Roles of MiR-372-3p in Proliferation of Hepatocellular
 Carcinoma Cells) อ.ที่ปรึกษาหลัก : อ. ดร.ชัยบุตร อริยะเชษฐ

มะเร็งเซลล์ตับเป็นมะเร็งระดับชนิดปฐมภูมิที่พบได้บ่อยที่สุด มะเร็งเซลล์ตับสามารถในการเพิ่มจำนวน
 ตัวเองได้แบบไม่มีที่สิ้นสุด รวมไปถึงเพิ่มจำนวนเซลล์ที่เป็นอมตะได้ ยิ่งไปกว่านั้น โปรตีนหลากหลายชนิดที่
 ควบคุมวัฏจักรของเซลล์ก็ยังคงถูกค้นพบด้วยว่ามีการแสดงออกผิดปกติในเซลล์มะเร็งเหล่านี้ จากการศึกษาเมื่อไม่
 นานมานี้ มีการค้นพบอาร์เอ็นเอชนิดหนึ่งที่ไม่ถูกถอดรหัสเป็นโปรตีน ชื่อว่าไมโครอาร์เอ็นเอซึ่งมีบทบาท
 หลากหลายในทางชีววิทยา ไมโครอาร์เอ็นเอบางชนิดสามารถเร่งหรือยับยั้งการเจริญเติบโตของเซลล์มะเร็งได้ผ่าน
 การมีปฏิสัมพันธ์กับเอ็มอาร์เอ็นเอเป้าหมายของมัน ตัวอย่างเช่น ไมโครอาร์เอ็นเอสามเจ็ดสองสามพีที่ได้มี
 การศึกษามากมายมาแล้วในมะเร็งลำไส้ มะเร็งทวารหนัก และมะเร็งสมอง เป็นต้น แต่บทบาทหน้าที่ของไมโคร
 อาร์เอ็นเอชนิดนี้ยังไม่ได้รับการศึกษามากนักในเซลล์มะเร็งตับ โดยเฉพาะเรื่องการควบคุมการเพิ่มจำนวนเซลล์
 ดังนั้นการทดลองนี้จึงได้นำเวกเตอร์ที่ใช้เพิ่มการแสดงออกของไมโครอาร์เอ็นเอสามเจ็ดสองสามพีใส่เข้าไปใน
 เซลล์มะเร็งตับเพื่อวัดการเพิ่มจำนวนของเซลล์ ผลการทดลองพบว่าเซลล์ตับทั่วไปมีการแสดงออกของไมโครอาร์
 เอ็นเอชนิดนี้มากกว่าเซลล์มะเร็งตับ อัตราการเพิ่มจำนวนเซลล์มะเร็งตับที่ถูกเพิ่มการแสดงออกของไมโครอาร์
 เอ็นเอชนิดนี้ยังลดลงด้วยโดยมีจำนวนเซลล์ที่เข้าสู่ระยะ S ในวัฏจักรของเซลล์นี้ลดลง จากการวัดระดับเอ็มอาร์
 เอ็นเอก็พบว่าส่วนใหญ่ที่ทำหน้าที่ควบคุมการเปลี่ยนผ่านเข้าสู่ระยะ S นั้นมีการแสดงออกที่เปลี่ยนแปลงไปเมื่อ
 เทียบกับเซลล์มะเร็งตับธรรมดา นอกจากนี้ก็ยังพบว่าไมโครอาร์เอ็นเอสามเจ็ดสองสามพีสามารถจับกับเอ็มอาร์
 เอ็นเอของ CCND1 ได้ จึงลดการแสดงออกของโปรตีน cyclin D1 ได้ด้วยเช่นกัน ดังนั้นจึงสรุปได้ว่าไมโครอาร์
 เอ็นเอสามเจ็ดสองสามพีจับกับเอ็มอาร์เอ็นเอของโปรตีน cyclin D1 แล้วยับยั้งการแปลรหัสเป็นโปรตีนก่อนจะ
 จะลดการเข้าสู่ระยะ S ของวัฏจักรของเซลล์ตามลำดับ

จุฬาลงกรณ์มหาวิทยาลัย
 CHULALONGKORN UNIVERSITY

สาขาวิชา ชีวเคมีทางการแพทย์
 ปีการศึกษา 2565

ลายมือชื่อนิสิต
 ลายมือชื่อ อ.ที่ปรึกษาหลัก

6470044030 : MAJOR MEDICAL BIOCHEMISTRY

KEYWORD: MicroRNA, MiR-372-3p, Cell cycle, Hepatocellular carcinoma, Cyclin D1

Pannathon Thamjamrassri : Exploring Roles of MiR-372-3p in Proliferation of Hepatocellular Carcinoma Cells. Advisor: CHAIYABOOT ARIYACHET, Ph.D.

Hepatocellular carcinoma (HCC) is the most common type of primary liver cancer. HCC has a replicative immortality and sustained proliferation rate. In addition, cell cycle-related protein regulating proliferation in cancer are often found dysregulated, allowing cancer cells to proceed their proliferation uncontrollably. Recently, a small non-coding RNA, microRNA (miRNA), was found to play an important role in numerous biological functions. Specific miRNA may ameliorate or promote cancer progression through different target mRNA. MiR-372-3p has been explored in various cancers such as colon cancer, colorectal cancer, and glioma. However, its functions have been rarely studied in HCC, especially in the aspect of cancer proliferation. This study, thus, aims to investigate its role in HCC cell line proliferation by introducing miR-372-3p overexpression vector into these cell lines. Results indicated that normal hepatocyte exhibited higher expression of miR-372-3p compared to that of HCC cells. Decelerated proliferation rate was detected in miR-372-3p overexpressing HCC cells. BrdU incorporation assay also indicated that miR-372-3p expression in HCC cells interfere the transition from G1 to S phase. G1-S phase cell cycle-related mRNA expression was different in miR-372-3p overexpressing cells compared to that of control. Dual-luciferase assay revealed that CCND1 was one of the miR-372-3p target mRNAs. Moreover, cyclin D1 protein level in miR-372-3p overexpressing cell lines was found downregulated compared to that of control. Therefore, it can be concluded that miR-372-3p interacts with CCND1 mRNA to prevent translation and to impede the cell cycle progression from G1 to S phase in HCC cell lines.

Field of Study: Medical Biochemistry

Student's Signature

Academic Year: 2022

Advisor's Signature

ACKNOWLEDGEMENTS

Firstly, I would like to sincerely thank my advisor, Asst. Prof. Chaiyaboot Ariyachet, Ph.D. for his precious advices. I am so grateful for his attention to this study.

I would like to express gratitude to my thesis committees, Naphat Chantaravisoot, Ph.D., Pornchai Kaewsapsak, Ph.D., and Asst. Prof. Woranop Sukpasangsi, Ph.D. for all the useful suggestion for this study.

I also appreciate the help from my 724 lab partners for providing the solution when facing technical and experimental difficulties.

I would like to thank my beloved parents, my sister, my cats, and my friends for their physically and mentally support throughout the period of this thesis.

Finally, I would like to thank to myself for all the efforts put into this study and for not ceasing to make such efforts.

Pannathon Thamjamrassri

TABLE OF CONTENTS

	Page
.....	iii
ABSTRACT (THAI).....	iii
.....	iv
ABSTRACT (ENGLISH).....	iv
ACKNOWLEDGEMENTS.....	v
TABLE OF CONTENTS.....	vi
LIST OF TABLES.....	x
LIST OF FIGURES.....	xi
Introduction.....	1
Research gap.....	3
Hypothesis.....	3
Research questions.....	3
Objectives.....	3
Research workflow.....	4
Literature review.....	5
Hepatocellular carcinoma (HCC).....	5
Cell cycle.....	7
MicroRNA (miRNA).....	9
MiRNA in HCC.....	12
MiR-372.....	15
Web-based bioinformatic Tools.....	16

Materials and methods.....	18
Materials and chemicals.....	18
Chemicals	21
Company	21
Roswell Park Memorial Institute (RPMI) 1640 medium	21
Gibco, Thermo Fisher Scientific, Massachusetts, USA.....	21
StripPRO™ 1 Min Stripping Buffer	21
Visual Protein, Taipei, Taiwan	21
T4 DNA ligase	21
New England Biolabs, Massachusetts, USA.....	21
Triton® X-100 Surfactant.....	21
OmniPur®, Calbiochem®, San Diego, USA.....	21
Tryptone Type-1 (Casitose Type-I).....	21
Himedia, Mharashtra, India.....	21
VisColor™ Pre-Stained Protein Marker.....	21
Visual Protein, Taipei, Taiwan	21
Yeast extract powder	21
Himedia, Maharashtra, India.....	21
Prediction of mRNA target.....	21
Plasmid construction.....	22
Enzyme digestion	23
Ligation.....	24
Gel electrophoresis.....	24
Transformation.....	24

Positive colony selection PCR.....	25
Plasmid extraction and purification	26
Transfection.....	27
Cell culture	27
MiRNA extraction and reverse transcription	28
MRNA extraction and reverse transcription	29
Quantitative Real time-polymerase chain reaction (qRT-PCR)	31
Dual luciferase reporter assay.....	33
Cell proliferation assay	33
MTT assay.....	33
BrdU assay.....	34
Cell counting.....	35
Protein extraction	35
Bradford assay	35
SDS-PAGE gel electrophoresis (Western Blot).....	36
Statistical analysis.....	37
Results.....	38
Web-based Bioinformatic Tools Revealed the Possible Interaction between MiR-372-3p and Cell Cycle-related Target MRNAs.....	38
Decreased MiR-372-3p Expression Was Found in HCC Cell Line.	41
PCR Product Verification.....	42
Selection of Established HCC Cell Lines.....	43
Transduced HCC Cell Lines Expressed a Higher Level of MiR-372-3p.	46

Changes in Cell Cycle-Related mRNA Were Detected in Established HCC Cell Line.	47
MiRNA-372-3p Decreased CCND1 MRNA Expression.	49
Deterred HCC Cell Line Proliferation as a Result of miRNA-372-3p Overexpression	50
Cyclin D1 Protein Expression Decreased in Transduced HCC Cell Line.....	53
DISCUSSION & CONCLUSION.....	54
REFERENCES	59
Appendixes	70
VITA.....	74



LIST OF TABLES

	Page
Table 1. Equipment used in this study.....	18
Table 2. Chemicals used in this study.....	20
Table 3. Primers used for miR-372 cloning.....	22
Table 4. PCR product digestion reagents.....	23
Table 5. pLVX-EF1 α -IRES-Puro digestion reagents.....	23
Table 6. pLVX-Ef α -IRES-Puro and PCR products ligation reagents.....	24
Table 7. Colony selection PCR reagents.....	25
Table 8. Time and temperature used in colony selection PCR.....	25
Table 9. MiRNA polyuridylation reagents.....	29
Table 10. MiRNA reverse transcription reagents.....	29
Table 11. CDNA synthesis reagents.....	30
Table 12. Time and temperature used mRNA reverse transcription.....	30
Table 13. qRT-PCR reagents.....	31
Table 14. Time and temperature used in miRNA qRT-PCR.....	31
Table 15. Time and temperature used in mRNA qRT-PCR.....	32
Table 16. Primers for qRT-PCR.....	32
Table 17. Overall web-based bioinformatic program prediction of candidate cell cycle related genes.....	39

LIST OF FIGURES

	Page
Figure 1. Spectrum of NAFLD and risk factors to HCC (48)	7
Figure 2. Cell cycle and its primary regulatory proteins (67).....	9
Figure 3. MiRNA biogenesis (canonical pathway) (7).....	11
Figure 4. An overview of the cell cycle-related proteins under the regulation of miRNAs (100).....	14
Figure 5. Prediction of cell cycle-related gene and miR-372-3p from each web-based bioinformatic program.	40
Figure 6. MiR-372-3p expression in THLE-2, JHH-4, and HepG2 cell line.	41
Figure 7. Verification of constructed LVX-EF1a-miR-372 vector.....	42
Figure 8. Puromycin selection of MiR-372-3p overexpressing HepG2.....	43
Figure 9. Puromycin selection of MiR-372-3p overexpressing JHH-4.	44
Figure 10. Puromycin selection of MiR-372-3p overexpressing SNU-449.	45
Figure 11. The expression of miR-372-3p in different transduced HCC cell lines.....	46
Figure 12. Cell cycle related-mRNA expression in miR-372-3p overexpressing HCC cell lines.	48
Figure 13. Dual-luciferase assay indicated that miR-372-3p targets CCND1 3'-UTR.	49
Figure 14. The proliferation rate was reduced in miR-372-3p overexpressing cell line.	50
Figure 15. BrdU incorporation assay of transduced HepG2.	51
Figure 16. BrdU incorporation assay of transduced SNU-449.....	52
Figure 17. Western blot of miR-372-3p overexpressing HepG2 and JHH4 indicates the amount of cyclin D1.	53

Figure 18. Proposed mechanism of miR-372-3p/CCND1 in HCC cells..... 58



Introduction

Hepatocellular carcinoma (HCC), one of the most common liver malignancies, is currently leading to cancer-related death occurring worldwide. It was also reported as the ninth cause of cancer deaths in USA and as the fourth globally (1, 2). Hepatitis virus infection, nonalcoholic steatohepatitis (NASH), obesity, liver fibrosis, and chronic liver diseases are the essential risk factors leading to HCC (3, 4). Several internal factors have been discovered to positively influence HCC development, such as changes in cellular microenvironment, interactions between non-viral and viral risk factors, genetic mutations, modulation of immune cells, and severity of the ongoing chronic liver disease (4).

Developed by Weinberg, cancer hallmarks represent many unique characteristics including sustaining proliferative signaling, evading growth suppressors, and enabling replicative immortality. Unlike normal cell that tightly regulated by growth-signals to maintain the balance in cell number, cancer cell becomes independent from those growth-signals (5). To facilitate limitless cell growth, cell cycle-related proteins are found to be overexpressed in cancer cells such as cyclin D, -E, and cyclin-dependent kinase (CDK) 2, -4, -6. Nevertheless, previous studies showed that tumorigenesis can be impaired by carcinogenic treatment or genetic manipulation. By targeting CDK 4 and CDK6, which is required to maintain cancer homeostasis, tumorigenesis could be impaired (6).

Recently, a non-coding RNA with 18-24 nucleotides length, micro-RNA (miRNA), was discovered to serve an important role in several biological activities including cell growth, cell proliferation, or apoptosis (7). Mechanistically, miRNA binds to mRNA target to either modulate upregulation or downregulation of the target (8, 9). Several miRNAs have been identified to be strongly involved with HCC pathogenesis, some of which are carcinogenic miRNAs or anti-carcinogenic miRNAs. For example, miR-181c-5p, miR-151, and miR-221-3p are classified as carcinogenic miRNAs (10-12), whereas

miR-199, miR-29, and miR-26b-5p are included in anti-carcinogenic miRNAs (13-15). Interestingly, numerous number of miRNAs has been known to modulate cancer progression through cell cycle-related proteins. To illustrate, miR-125b targets CDC25A, and E2F3 to initiate cell cycle arrest at G1/S transition. However, downregulation of miR-125b is often found in many types of cancer including glioma stem cells, and bladder cancer (16, 17). In pituitary adenoma, miR-128a, miR-155, and miR-516a-3p were found to suppress Wee1 kinase which is required to delay mitosis. These miRNAs are thus considered as anti-carcinogenic miRNAs (18).

Liver fibrosis and its later stage, liver cirrhosis, can lead to the development of HCC (19). Residing within the space of Disse, hepatic stellate cells (HSCs) remain in quiescent state and feature several retinoid lipid droplets (20). Hepatocyte injury resulting from toxic or viral infection triggers the alteration of HSC phenotype into collagen-producing myofibroblasts or activated HSC (20). In response to hepatocyte injury, myofibroblasts migrate to the site of injury and secrete extracellular matrix (ECM), forming liver nodules and disrupting liver architecture (20). Integrative miRNA-mRNA interaction study revealed miRNA-372 was in the top 10 genes that were found to be downregulated in activated HSC (21).

MiR-372 has been widely investigated in many cancers such as prostate cancer, colon cancer, colorectal cancer, and HCC (22-25). However, its role in HCC proliferation has not been fully elucidated, especially in the aspect of cell cycle regulation. This study aims to discover the underlying function of miR-372-3p in modulating cancer progression through cell-cycle related protein. By using the web-based bioinformatic tools such as TargetScan, miRTarBase, mirSystem, and DIANA-microT, the possible mRNA targets could be predicted.

Research gap

- 1.1. An interaction between miR-372-3p and cell cycle related mRNA has not been explored.

Hypothesis

- 1.2. MiR-372-3p might play an important role in regulating HCC cell cycle progression.

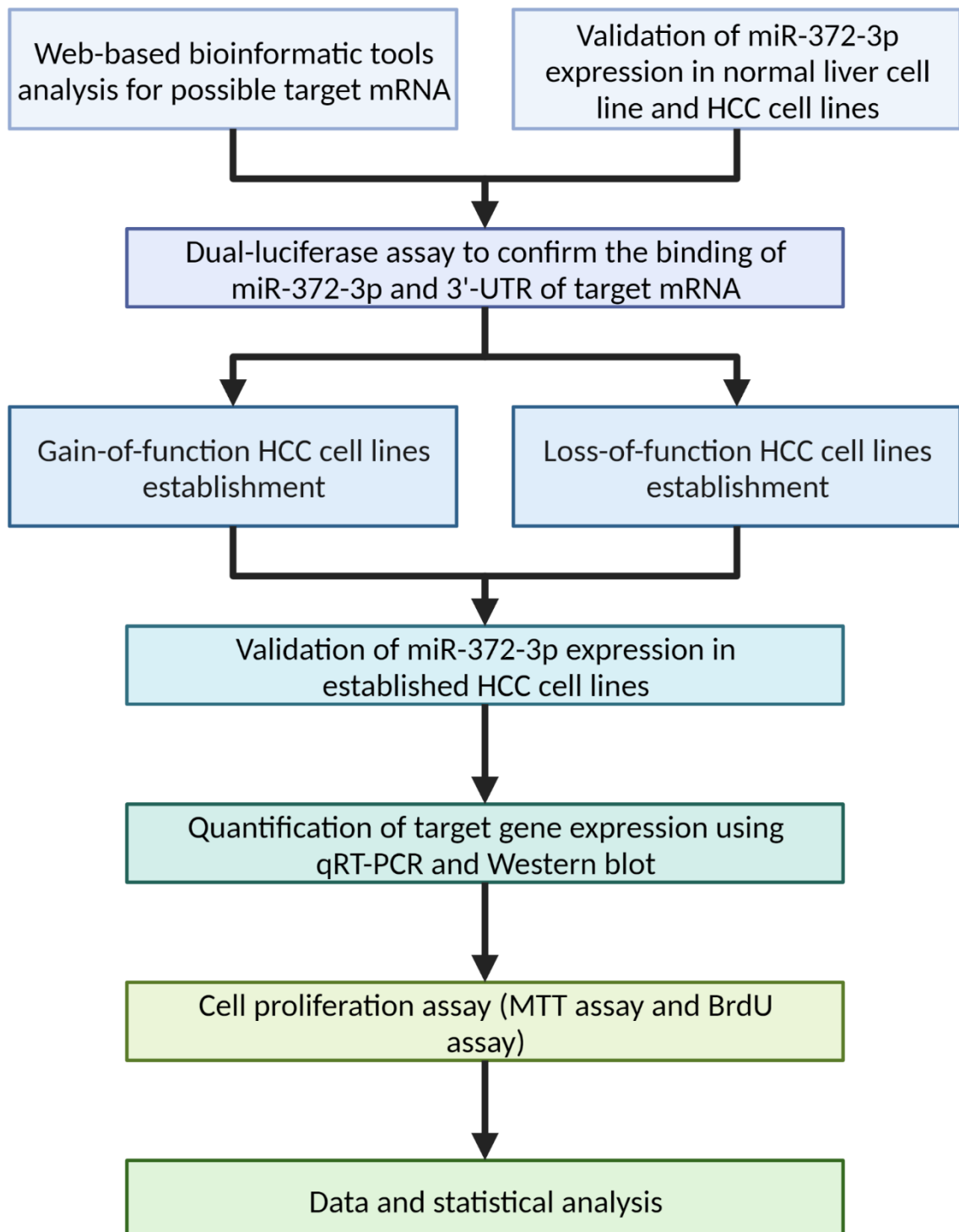
Research questions

- 1.3. Does miR-372-3p show a differential expression between normal liver cell line and HCC cell line?
- 1.4. Does miR-372-3p modulate HCC proliferation through cell-cycle related protein?

Objectives

- 1.5. To investigate the differential expression of miR-372-3p in normal liver cell line and HCC cell lines
- 1.6. To explore the cell-cycle related functions of miR-372-3p in HCC cell lines

Research workflow



Literature review

Hepatocellular carcinoma (HCC)

HCC is the fourth common leading cause of cancer-related death worldwide, especially in the country where medical resources and quality of lifecare have been limited, such as, sub-Saharan Africa and Eastern Asia (2, 26). From 2005 to 2015, HCC was the second underlying cause of death, after lung cancer (2, 26). In recent studies, forty-four percent of patients diagnosed with HCC were found to harbor a mutation in *TERT* promoter which regulates the transcription of telomerase catalytic subunit (27). Interestingly, hepatitis B virus (HBV) genome insertion site is frequently located within *TERT* promoter (28). Mutation on β -catenin encoding gene, *CTNNB1*, and the cell cycle regulator gene, *TP53*, were also associated to clinical characteristics of HCC progression, with 27-40% and 21-31% of patients diagnosed with HCC, respectively (27, 29). Moreover, *MET*, *MYC*, *VEGFA*, *FGF19*, and *CCND1* chromosomal amplifications also contribute to the activation of multiple oncogenic signaling pathways (30). In smaller scale, single nucleotide polymorphisms (SNP) in patatin-like phospholipase domain containing 3 (*PNPLA3*) are highly correlated to HCC (31).

Infection of hepatitis B and C virus (HBV, HCV) is the major contribution to HCC pathogenesis, up to 80% of HCC patients worldwide (32, 33). African and Eastern Asian countries were reported to be mostly affected by HBV infection whereas northern Africa was majorly affected by HCV infection instead (34, 35). Several studies have demonstrated that individual harboring hepatitis B virus has 10-25% lifetime risk to develop HCC (36). Different mechanisms are utilized by hepatitis virus in driving HCC development. These mechanisms include the induction of oxidative stress mediated by consistent inflammation and immune system regulation, intracellular oxidative stress damage mediated by viral proteins, and alteration of signaling pathways by viral protein (37). Many viral products of HBV, such as X protein (HBx), surface proteins (HBsAg), core antigen (HBcAg), and excreted e antigen (HBeAg) modulate host cellular machinery to reinforce cancer hallmarks (37, 38). For

example, HBx downregulates p53, a tumor suppressor, to promote cell proliferation (5, 37). HBsAg induces oxidative stress in endoplasmic reticulum, resulting in inflammation and genomic instability, respectively (39, 40). Similar to HCV, its encoded products include core protein, E1, E2, NS2, NS3, NS4A, NS4B, NS5A, and NS5B which were found to promote cancer hallmarks (37, 41). To illustrate, NS4B enhances ER stress (42) whereas NS5A suppresses PTEN to allow cell growth (43). Nevertheless, hepatitis viral infection alone is not sufficient to develop HCC as other factors are also required (44). HBV possesses 10 genotypes whereas HCV contains 6 genotypes (32). Genotype B and C of HBV with mutation on T1762/A1764 basal core promoter were reported to strongly drive HCC progression in individuals younger than age 50. In Asia, genotype C is associated with HCC and other severe liver diseases more than genotype B (45). In southeast Asia, HCV genotype 3 infection has more potential risk to develop HCC than genotype 1 (46).

Another contributor that leads to HCC is nonalcoholic fatty liver disease (NAFLD). NAFLD contains a broad spectrum of many liver diseases including nonalcoholic steatohepatitis (NASH), nonalcoholic fatty liver (NAFL) and liver fibrosis and cirrhosis (47). NAFL features steatosis, an excessive triglyceride accumulation in hepatocytes, and could develop into NASH, a following phase that exhibits hepatocyte injury and mild inflammation. In addition, both NAFL and NASH have a potential to influence the formation of liver fibrosis and cirrhosis and ultimately HCC (48).

Diabetes mellitus has been known as an independent cause leading to HCC pathogenesis without the requirement of the other risk factors (49). This metabolic disease exhibits an imbalance in insulin and blood sugar level. Hyperinsulinemia, a remarkable characteristic of diabetes, elevates the expression of insulin-like growth factor 1 (IGF-1) which further stimulates cell proliferation (49, 50). Excessive insulin and glucose also trigger the biosynthesis of type I procollagen mRNA in hepatic stellate cells, stimulating liver fibrosis (51). Type 2 diabetes is positively associated with obesity which facilitates the secretion of inflammatory cytokines from visceral

adipose tissue, promoting carcinogenesis (50). With hyperglycemia condition, carcinogenic potential could be readily increased from the glycosylation of hemoglobin (50, 52). Iron releasing resulted from glycosylated hemoglobin can be utilized as a substrate for free radical generation which causes oxidative stress (53).

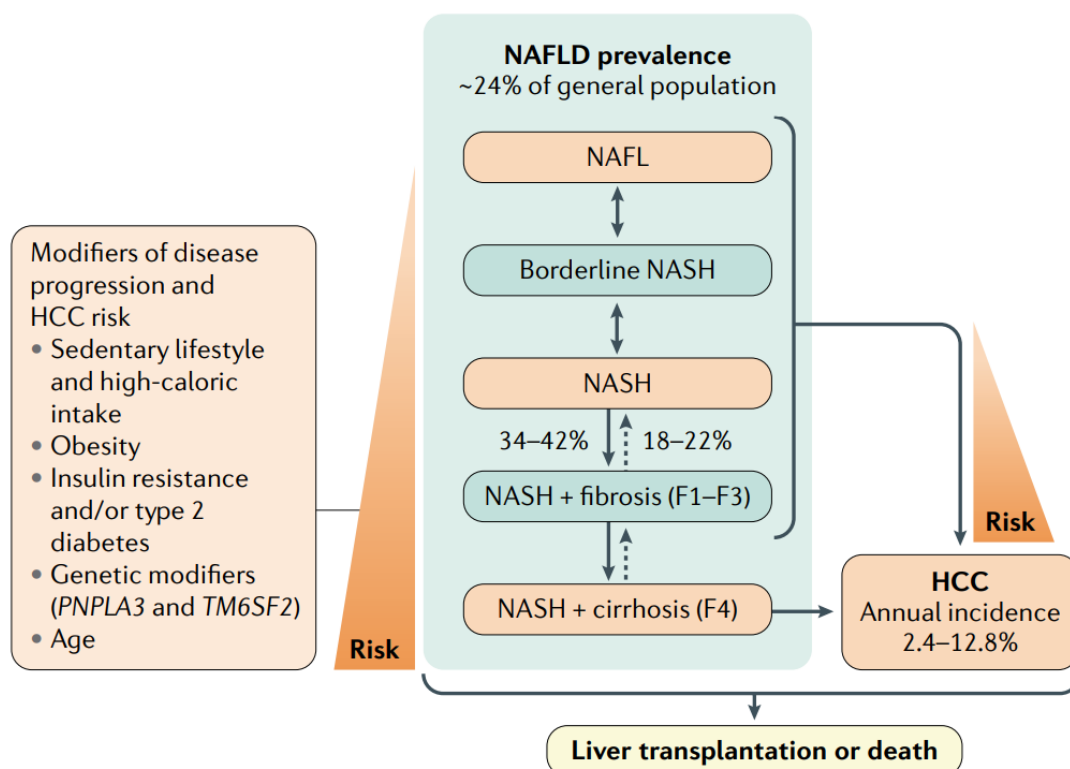


Figure 1. Spectrum of NAFLD and risk factors to HCC (48)

Cell cycle

Cell cycle is divided into four principal phases: G1, S, G2, and M phase. G1, S, and G2 phase are included in sub-phase interphase, whereas M phase can be further divided into mitosis and cytokinesis. There are five states in mitosis: prophase, prometaphase, metaphase, anaphase, and telophase (54, 55). However, cells can also leave the cell cycle to quiescent state, G0 phase, in serum-starved condition or in high-confluence density (56, 57). The transition to the next phase and the progression of the cell cycle is primarily regulated by cyclin dependent kinase (CDK) and cyclin. CDK, a kinase controlled by the phosphorylation at tyrosine and

threonine residues, forms a complex with cyclin to either becomes activated or inactivated, depending on the type of cyclin they associated (58).

During the G1 phase, CDK4 or CDK6 associate with cyclin D, establishing a cyclin D-CDK4/6 complex, to activate the complex and further partially phosphorylates downstream substrate, retinoblastoma protein (RB) (59, 60). The phosphorylation of RB leads to the detachment of its target, E2F, which is a critical transcription factor in facilitating early cell cycle genes (61). Detached E2F upregulates the expression of cyclin A and cyclin E. CDK2 joins cyclin E to form a cyclin E-CDK2 complex and then fully phosphorylates RB, respectively, allowing cell to proceed to the S phase (60). In the S phase, cyclin A binds to CDK2 to establish a cyclin A-CDK2 complex which is required to stimulate the proteins responsible for DNA synthesis (62). After entering the G2 phase, cyclin B-CDK1 complex gradually increases from the beginning to the end of the phase. The rising of cyclin B-CDK1 complex, maintained by cyclin A-CDK1 complex, drives cell cycle to the M phase. Cyclin B-CDK1 complex starts to decline continuously throughout the M phase, promoting the completion of mitosis (63).

In order to be tightly regulated, cyclin and CDK, in turn, are controlled by several cell cycle inhibitors such as inhibitors of CDK4 (INK4) family and Cip/Kip protein family. The INK4 family consists of p16^{INK4a} (Cdkn2a), p15^{INK4b} (Cdkn2b), p18^{INK4c} (Cdkn2c), and p19^{INK4d} (Cdkn2d). Cip/Kip protein family, an inhibitor to cyclin, includes p21 (Cdkn1a), p27 (Cdkn1b), and p57 (Cdkn1c) (64). Inducing INK4 expression ceases the cell cycle at G1 phase by binding to CDK4 or CDK6 and thus leading to the degradation of cyclin D. In contrast, Cip/Kip protein stabilizes cyclin D-CDK4 complex and binds to cyclin E-CDK2 to inactivate the complex, preventing it from driving cell cycle to S phase (59). However, the inhibitory effects of these inhibitors are tampered in cancer cell as a result from the mutation or inactivation of tumor suppresser encoding genes or the upregulation of oncogenes that further activate cyclins-CDKs complex (65). In HCC, 5' CpG island of p16^{INK4a} encoding gene is often found to be

hypermethylated, leading to the reduced expression level of p16^{INK16a}, as a result from the elevated expression of DNA methyltransferases, DNMT1 and DNMT3A (66).

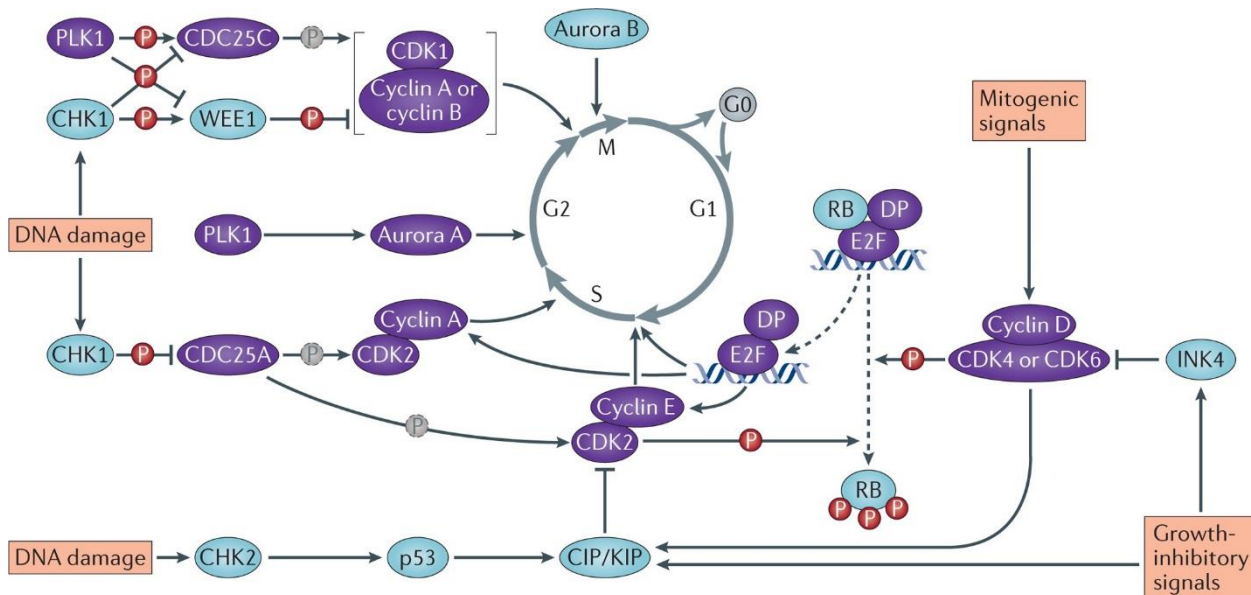


Figure 2. Cell cycle and its primary regulatory proteins (67)

MicroRNA (miRNA)

MiRNA was found in 1993 by Lee and colleagues while studying developmental timing of *Caenorhabditis elegans*, a nematode (68). Following studies revealed that miRNA is a non-coding RNA with 18-24 nucleotides in length and it acts as post-transcriptional regulator, controlling gene expression. The biogenesis of miRNA usually initiates with transcription by RNA polymerase II, yielding primary miRNA (pri-miRNA), before entering hairpin-like structure formation via canonical pathway using Drosha protein. This hairpin-like structure, precursor miRNA (pre-miRNA), is then exported to the cytoplasm and further processed by Dicer to cleave hairpin loop, resulting in imperfect miRNA duplexes. Cleaved miRNA duplexes interact with Argonaute family proteins including Ago 1-4 to establish a miRNA-induced silencing complex (miRISC), in which strand selection takes place (69, 70). However, miRNA can also be produced via multiple non-canonical pathways. For instance, pri-miRNA is cleaved by Drosha-DiGeorge Syndrome Critical Region 8 (DGCR8) complex and exported to cytoplasm by exportin 5, respectively (71). The exported pre-miRNA then

joins Ago 2 and Dicer to form miRISC (72). In another example, pre-miRNA is capped with 7-methylguanosine (m^7G) and is exported from nucleus using exportin 1 without cleavage (73).

The mechanism of miRNA-mediated post-transcriptional regulation has been extensively studied. They were reported to promote or silence gene expression (8, 9). For gene silencing in eukaryotes, miRISC binds to miRNA response elements (MREs) of its mRNA target through imperfect-base pairing (74, 75). GW182 family protein is recruited to bind to Ago and acts as an adaptor protein (76). Poly(A)-deadenylase complex PAN2-PAN3 and CCR4-NOT, effector proteins that mediate poly(A)-deadenylation, subsequently join GW182 to interact with Ago (9, 77). Decapping is then proceeded by decapping protein 2 (DCP2) and exoribonuclease 1 (XRN1) begins to degrade target mRNA in 5'-3' direction, ultimately silencing gene expression (74). In contrast, fragile-x-mental retardation related protein 1 (FXR1) and miRNA-protein complex (microRNPs) interact to 3'-untranslated region (3'-UTR) of the target mRNA to stimulate translation (78). Another example, binding of miRNA to 5'-UTR can also activate ribosomal protein translation (79). However, gene upregulation mediated by miRNA is suggested to take place under specific conditions such as in serum or amino acid-starved, in cell cycle arrest stage, and in quiescent phase of oocyte (78-81).

Several biological processes, such as cell metabolism, cell proliferation, cell apoptosis, cell necrosis, and epithelial-mesenchymal transition (EMT) in cancer, have been known to be modulated by miRNAs (7). For example, miR-338-3p was found to be negatively correlated with myelin transcription factor 1-like (MYT1L) which involves with cancer and neurodegeneration (82). Overexpression of miR-338-3p inhibits cell proliferation, cell migration, and cell invasion and stimulates apoptosis in glioma cells. Therefore, miR-338-3p might modulate these processes through miR-338-3p/MYT1L axis (83). In prostate cancer cell line, overexpression of miR-29b-3p suppresses cell proliferation and promotes the expression pro-apoptotic protein Bim (84). By downregulating secreted phosphoprotein 1 (SPP1), miR-27a-3p could

ameliorate systemic sclerosis in skin and lung. SPP1 was identified as a fibrosis promoter in many organs, and it regulates signaling pathway through ERK1 and ERK2 (85). Collectively, miR-27a-3p/SPP1/ERK1/2 axis are crucial for inhibiting skin and lung fibrosis (86). Although, some miRNAs were found to promote cancer progression. Both upregulated miR-200b and miR-200c in colorectal cancer interfere the expression of reversion-inducing cysteine-rich protein with Kazal motifs (RECK), a cell cycle suppresser, to promote cell proliferation (87). MiR-21 acts as an oncogene in many types of cancer, supporting cell proliferation, cell migration, and cell invasion. In addition, it also fortifies the resistance to chemotherapy and radiation (88). In non-

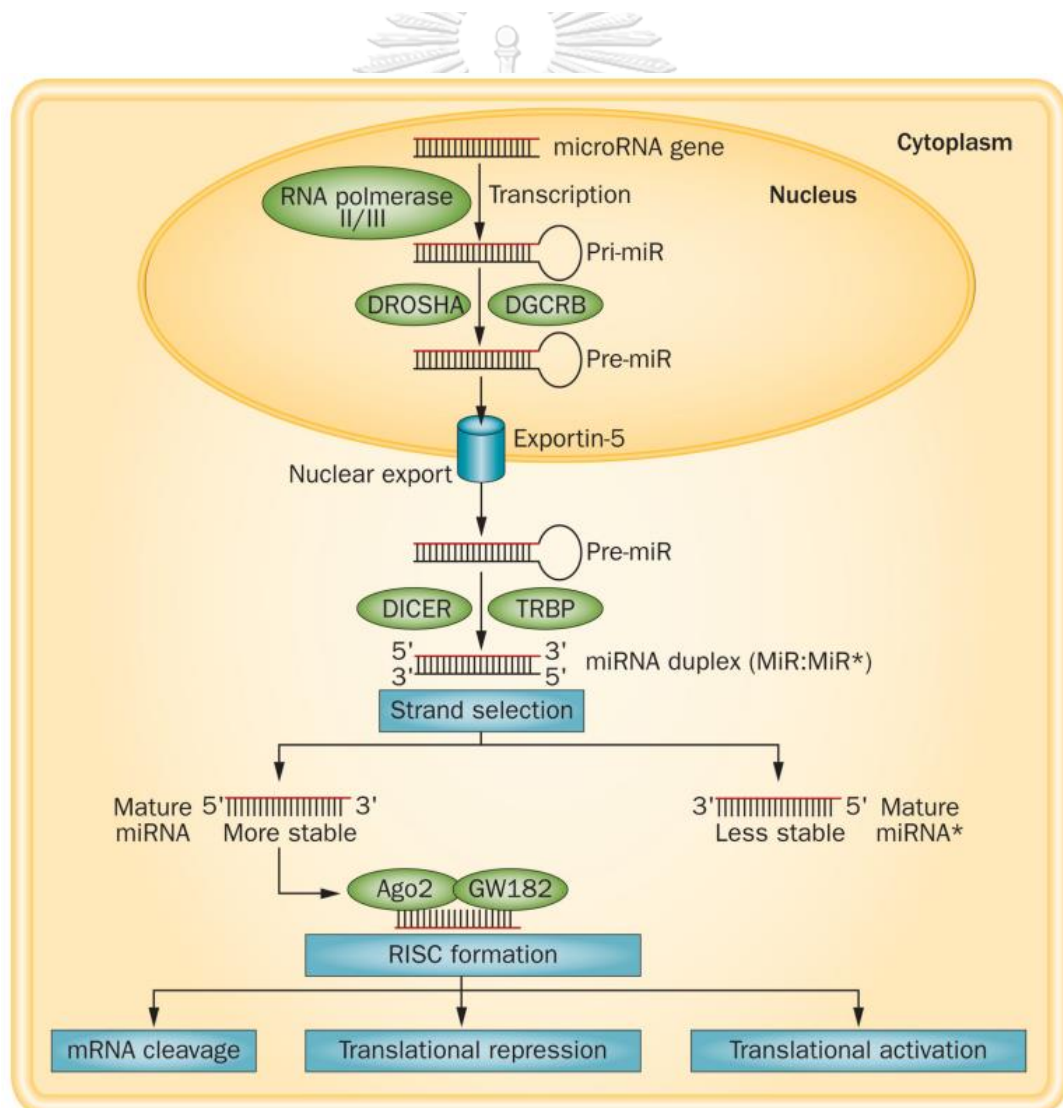


Figure 3. MiRNA biogenesis (canonical pathway) (7)

small cell lung cancer, miR-224 actively promotes cell proliferation, cell migration, and cell invasion by targeting SMAD4 and TNF α -induced protein 1 (TNFAIP1) (89).

MiRNA in HCC

A numerous number of miRNAs have been shown to be involved with HCC pathogenesis. Some of them support HCC progression, while the others ameliorate or suppress HCC development. MiR-181c-5p has an oncogenic role in HepG2. It downregulates F-box and leucine-rich repeat protein 3 (Fbxl3), promoting cell apoptosis and inhibits cell proliferation, cell migration, and cell invasion (10, 90). MiR-616 suppresses phosphatase and tensin homolog (PTEN) to support HCC cell line migration, invasion, and EMT (91). PTEN acts as a tumor inhibitor by preventing PI3K/Akt signaling pathway which influences cancer growth (92). The overexpression of miR-151 and focal adhesion kinase (FAK), positively correlates with intrahepatic metastasis of HCC. Mechanistically, miR-151 targets RhoGDI, a metastasis inhibitor, and synergistically functions with FAK to promote metastasis (11). As found upregulated in HCC, miR-221-3p represses leukemia inhibitory factor receptor (LIFR) by binding to its 3'-UTR. LIFR has been described as a tumor suppressor in many cancers, and thus inhibiting its functions lead to enhancement in cancer cell activities (12). Furthermore, recent studies have revealed several miRNAs involved in HCC progression including miR-17-92, and miR-181 (69).

By regulating through various targets, miR-199 has an anti-oncogenic role in HCC. For example, miR-199 binds to 3'-UTR of Regulators of G-protein signaling 17 (RGS17) mRNA, preventing transcription. RGS17 was previously reported to facilitate cancer proliferation, migration, and invasion (13). X-box binding protein 1 (XBP1) mRNA, a promoter of cell proliferation through cyclin D, was also identified as another target of miR-199 (93). Moreover, miR-199 was shown to downregulate Notch1 and R-cadherin and thereby inhibiting EMT (94). MiR-29, a tumor suppresser miRNA, directly binds to 3'-UTR of ribosomal protein s15a (RPS15A), which is known to be associated with the development of many cancers. In addition, cyclin D1 and cyclin A were

downregulated whereas p21 was upregulated when overexpressed with miR-29, impeding cell cycle progression and cell proliferation (14). MiR-26b-5p also plays an important role as anti-cancer miRNA. Through suppressing matrix metalloproteinase 2 (MMP2), Snail, and vascular endothelial (VE)-cadherin, miR-26b-5b could inhibit tumor angiogenesis and cell proliferation (15). Additional anti-tumor miRNAs have been studied and described, such as let-7, miR-26, miR-101, and miR-122 (69).

Previous studies have indicated several cell cycle protein targets of miRNA in HCC. Overexpression of miR-124 or miR-203 in HCC cell lines revealed many downregulated target proteins including CDK6, suggesting its role as an anti-cancer miRNA (95). By targeting 3'-UTR of p21Cip1/Waf1, oncogenic miR-423 drives cell cycle progression from the G1 to S phase and stimulates HCC growth (96). As found upregulated in HCC, miR-221 binds to 3'-UTR CDKN1B/p27 and CDKN1C/p57, a cyclin-dependent kinase inhibitor (CDKI), to increase the number of cell in the S phase and promote cell proliferation (97). Silencing effect to cyclin D1, CDK6, and E2F3 can be found after the overexpression of miR-195 in HCC cell line, inhibiting the transition from the G1 to S phase (98). Knock-down of miR-106b-25 cluster including miR-25, miR-93, and miR-106b, leads to the upregulation of E2F1, and thus deters HCC proliferation and anchorage-independent growth (99).

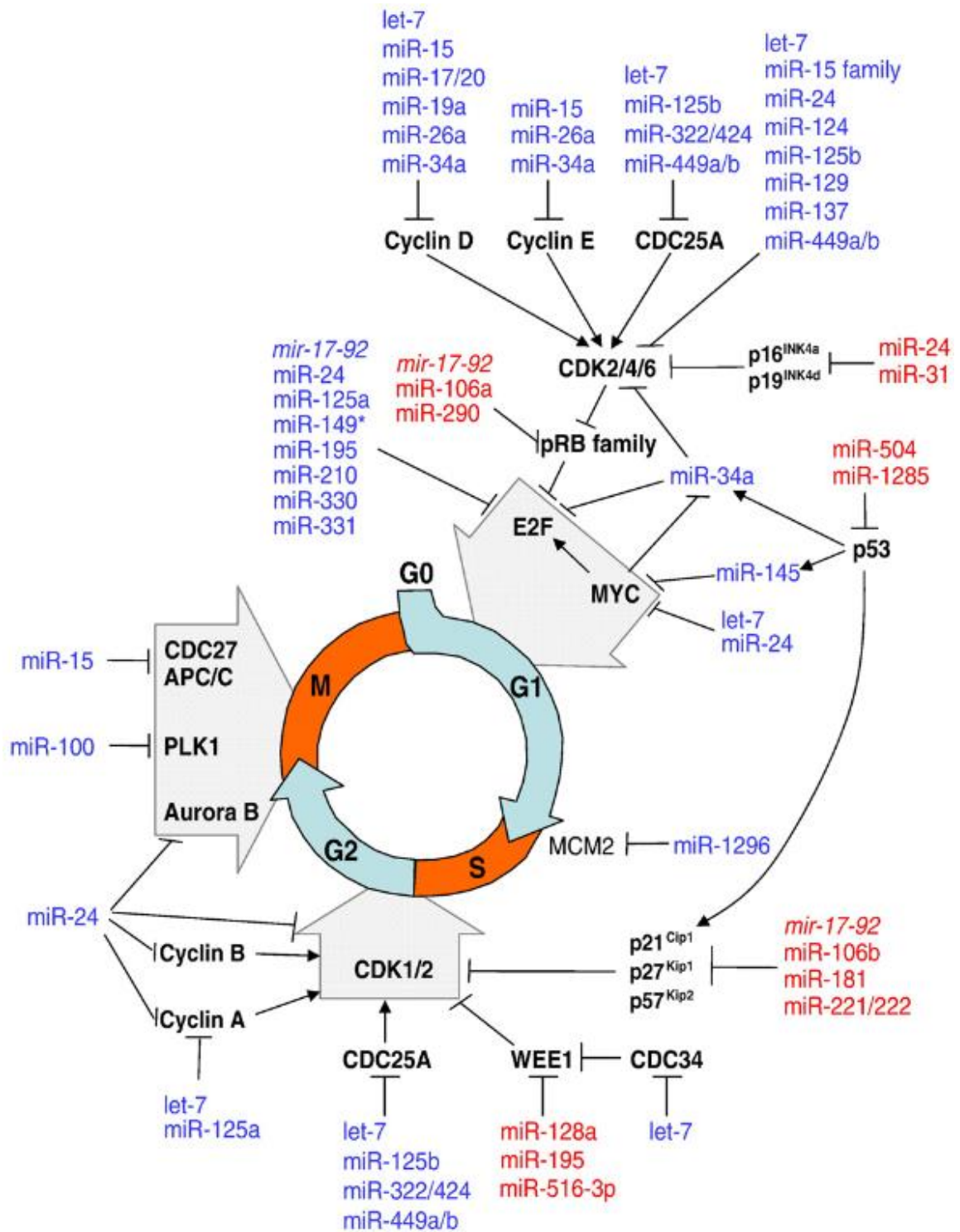


Figure 4. An overview of the cell cycle-related proteins under the regulation of miRNAs (100)

MiR-372

Transcribed from the MiR-371-372 gene cluster on chromosome 19q13.42, miR-372 has been known to be involved with many cancer cell activities such as cell proliferation, cell migration, cell invasion, and apoptosis. MiR-372 may serve as either oncogenic miRNA or anti-oncogenic miRNA in a particular type of cancer (101). In addition, miR-372 has also been shown to correlate with poor prognosis in glioma and HCC (102, 103). Upregulating miR-372 indicated its role as oncogenic miRNA and may regulate aggressive development in gliomas (102). In contrast, miR-372 expression was downregulated in HCC tissue and was associated with low survival rate of patients diagnosed with HCC (103).

Previous studies have explored the mechanistic function and target mRNA of miR-372 in various cancers. To demonstrate, overexpression of miR-372 in breast cancer cell line, MCF-7, was reported to suppress cell proliferation and promote apoptosis by targeting 3'-UTR of E2F1 (101). In colon cancer cell line, miR-372-3p binds to 3'-UTR of MAP3K2, preventing the mediation of MAPK signaling and thus inhibiting cell proliferation (23). Inducing the expression of miR-372-3p in osteoblastic cell line could prohibit cell proliferation and cell metastasis via regulating FXRD domain-containing ion transport regulator 6 (FXRD6) (104). Interestingly, miR-372 was also found to target the same mRNA, large tumor suppressor kinase 2 (LATS2), in different cancers. Suppression of miR-372-3p mediates Hippo signaling through LATS2, which inhibits colorectal cancer proliferation, migration, and invasion (24). In similar scenarios, downregulation of miR-372 ceases breast cancer proliferation in the G1/S phase and increases apoptosis by targeting LATS2 (105). By suppressing miR-372-3p in lung squamous cell carcinoma cell line, fibroblast growth factor (FGF9) expression could be restored and inhibit cell proliferation and cell invasion (106). In HCC, silencing ATPase family AAA domain containing 2 (ATAD2) by overexpressing miR-372 could lead to cell cycle arrest in the G1 phase and therefore inhibit cell proliferation (25).

Web-based bioinformatic Tools

TargetScan was first developed by Lewis BP and colleagues in 2003 (107). The algorithm predicts the possible interactions between miRNA and target mRNA relying on thermodynamics-based modeling of RNA:RNA duplex interactions (107). Based on Watson-Crick base pairing principle, TargetScan searches UTR of the specific mRNA that match to base 2-8 of miRNA, seed region (107). Moreover, this bioinformatic tool also combines the use of RNAfold and RNAeval program in order to enhance specificity by integrating folding free energy G to the interaction sites (107). TargetScan mostly focuses on 5' end of miRNA, rather than on 3' end, since perfect complementary is required for seed region at 5' end (107).

Unlike TargetScan, MirTarBase does not predict the possible interactions between miRNA and mRNA (108). MirTarBase manually searches and collects research articles related to functional studies of miRNA such as reporter assay, western blot, microarray experiment, gain-of-function, and loss-of-function of miRNA (108). It categorizes the retrieved evidence into two main groups, according to the functional study utilized in the research article, including strong experimental evidence, and less strong experimental evidence (108). Using western blot, qPCR, and luciferase reporter assay under the conditions of gain-of-function or loss-of-function are classified as strong experimental evidence (108). However, employing high-throughput identification methods such as pSILAC, and microarray are included in less strong experimental evidence since such method does not require the miRNA presence (108).

Recently developed, mirSystem integrates numerous analyses and other bioinformatic programs to predict the interactions between miRNA and mRNA (109). First, the program converts miRNA ID before integrating several other bioinformatic tools, such as DIANA-microT, miRanda, miRBridge, TargetScan, TarBase, miRecords, to predict target mRNA (109). In addition, miSystem also combines Kyoto encyclopedia of genes and genomes (KEGG), Gene Ontology, and Biocarta to analyze the functional

and canonical pathway of miRNA. After statistical analyzing, the data is represented in the form of table and bar charts (109). mirSystem, however, faces its major challenge due to the inconsistency of miRNA IDs used throughout different algorithms and data sources (109). The challenge could be solved by using basic local alignment search tool (BLAST) to identify and retrieve miRNA and allowing user to put miRNA sequences as an input (109).

DIANA-microT mainly focuses on the 5' end of miRNA, seed region, that complementarily pairs to miRNA recognition elements (MRE) of target mRNA at UTR (110). The weighted sum of the scores of all determined MREs on the 3'-UTR will be used to calculate overall miTG score (110). DIANA-microT also combines the use of other analysis tools such as mirExTra for pre-processing tool, and mirPath for post-processing tool (110). Basically, mirExTra identifies miRNA that might relate to the changes of the transcriptome by listing the differentially express coding genes and the genes with unchanged expression (110). mirPath integrates KEGG pathways analysis to help uncover the biological pathways (110).



Materials and methods

Materials and chemicals

Table 1. Equipment used in this study.

Materials/Chemicals	Company
Autoclave (Hiclave HVA-85)	Hirayama, Kasukabe-Shi Saitama, Japan
Autopipette P10, P100, and P1000 μ l (Nichipet)	Nichiryō, Saitama, Japan
Blot transfer device (Trans-Blot SD Semi-Dry Transfer Cell)	Bio-Rad, California, USA
Cell culture 6-, 24-, and 96-well plate	Corning, New York, USA
Class II biohazard safety cabinet	Labconco, Kansas, USA
CO ₂ incubator (Forma Series 3 Water Jacketed)	Thermo Fisher Scientific, Massachusetts, USA
Cryotube	Sigma Aldrich, Missouri, USA
Distilled water producer	Thermo Fisher Scientific, Massachusetts, USA
Gel and membrane visualizer (UVP ChemStudio)	Analytik Jena, Jena, Germany
Horizontal electrophoresis system (Wide Mini-Sub [®] Cell GT, Mini-Sub [®] Cell GT)	Bio-Rad, California, USA
Microcentrifuge tubes	Axygen, California, USA
Microplate reader (Synergy [™] HTX multi-mode reader)	Biotek, Vermont, USA
Microscope (Leica DMI1) (EVOS [™] FL Auto 2 Imaging System)	Leica Biosystems, Wetzlar, Germany Invitrogen, Thermo Fisher Scientific, Massachusetts, USA
Nitrocellulose membrane	Amersham, Thermo Fisher Scientific, Massachusetts, USA
PCR tube	Extragene, Taichung, Taiwan

Materials/Chemicals	Company
Real-time thermal cycler (QuantStudio™ 3 Real Time PCR System)	Applied Biosystems, Thermo Fisher Scientific, USA
Spectrophotometer	Denovix, Delaware, USA
Sterile serological pipette 5-, and 10 ml	Thermo Fisher Scientific, Massachusetts, USA
Tabletop microcentrifuge (Centrifuge 5418R)	Eppendorf, Hamburg, Germany
Thermal cycler (Mastercycler® nexus SX1)	Eppendorf, Hamburg, Germany
Thermo shaker incubator (MTH-100)	Miulab, Hangzhou, China
Vortex mixer (Vortex-Genie 2)	Scientific Industries, New York, USA
Vertical electrophoresis system (Mini-PROTEAN tetra vertical electrophoresis cell)	Bio-Rad, California, USA

Table 2. Chemicals used in this study.

Chemicals	Company
3-(4,5dimethylthiazol-2-yl)-2,5-diphenyl tetrazolium bromide (MTT)	Invitrogen, Thermo Fisher Scientific, Massachusetts, USA
4X CAPITOL™ qPCR master mix	Biotechrabbit, Berlin, Germany
Antibiotic-Antimycotic (Anti-Anti) (100X)	Gibco, Thermo Fisher Scientific, Massachusetts, USA
Anti-mouse IgG, HRP-linked antibody	Cell Signaling Technology, Massachusetts, USA
Anti-rabbit IgG, HRP-linked antibody	Cell Signaling Technology, Massachusetts, USA
Bio-Rad Protein Assay Dye Reagent Concentrate	Bio-Rad, California, USA
BlockPRO™ 1 Min Protein-Free Blocking Buffer	Visual Protein, Taipei, Taiwan
BrdU (IIB5) sc-32323 mouse monoclonal antibody	Santa Cruz Biotechnology, Texas, USA
Dulbecco's Modified Eagle Medium (DMEM)	Cytiva, Massachusetts, USA
Eagle's Minimum Essential Medium (EMEM)	Gibco, Thermo Fisher Scientific, Massachusetts, USA
Fetal bovine serum (FBS)	Gibco, Thermo Fisher Scientific, Massachusetts, USA
GAPDH loading control monoclonal antibody (GA1R)	Invitrogen, Thermo Fisher Scientific, Massachusetts, USA
LB agar powder (Miller)	Bio Basic, Markham, Canada
LE agarose	Premium grade and Quality products, USA
Phosphate buffer saline (PBS) tablets	MilliporeSigma, Massachusetts, USA
Polyethylene glycol sorbitan monolaurate (TWEEN® 20 Vetec™, reagent grade, 40%)	Sigma Aldrich, Missouri, USA
Rb mAb to Cyclin D1 (SP4)	Abcam, Cambridge, UK

Chemicals	Company
Roswell Park Memorial Institute (RPMI) 1640 medium	Gibco, Thermo Fisher Scientific, Massachusetts, USA
StripPRO™ 1 Min Stripping Buffer	Visual Protein, Taipei, Taiwan
T4 DNA ligase	New England Biolabs, Massachusetts, USA
Triton® X-100 Surfactant	OmniPur®, Calbiochem®, San Diego, USA
Tryptone Type-1 (Casitose Type-I)	Himedia, Mharashtra, India
VisColor™ Pre-Stained Protein Marker	Visual Protein, Taipei, Taiwan
Yeast extract powder	Himedia, Maharashtra, India

Prediction of mRNA target

MRNA targets were predicted by web-based programs including TargetScan, miRTarBase, miRSystem, and DIANA-microT. The following cell cycle related genes were used in each database; CDK2/4/6, CCND1/2/3, CCNE1, E2F1/2/3/4/5/8, CDC25A, PCNA, and RB1.

‘Human’ species and ‘miR-372-3p’ were used as input data for TargetScan (https://www.targetscan.org/vert_80/). The program searches for conserved miR-372-3p sites and compares human gene sequences. After matching seed region of miR-372-3p to 3'-UTR of target genes, context score can now be calculated based on several features including the position of 3'-UTR, the additional base pairing other than seed region. Lower context scores indicate more favorable target sites.

As described earlier, miRTarBase (<https://mirtarbase.cuhk.edu.cn>) integrates published research articles or literature reviews involving with the specific miRNA and classified the evidence into two groups: strong experimental evidence, and less strong experimental evidence. ‘hsa-miR-372-3p’ was used as input data and the results were showed as a sum of total research articles that describe the interaction of hsa-miRNA-372-3p and the specific target gene. Higher number of research articles implies a strong evidence.

miRSystem (<http://mirsystem.cgm.ntu.edu.tw>) integrates many web-based bioinformatic programs to predict target mRNA. ‘miRNAs to Target Genes’ option was selected and ‘has-miR-372-3p’ was used as an input data. ‘KEGG’, ‘Biocarta’, ‘Pathway Interaction Database (human only)’, and ‘Reactome (human only)’ were selected as functional annotations. ‘Include validated genes greater than or equal to 3’ was selected as one of the parameters, allowing non-experimentally validated targets to be displayed. O/E (Observe/Expect) ratio was set at 2, and ‘Total genes in a pathway’ was set between 25 and 500 in order to focus on biological functions or pathways that consist of a minimum of 25 genes and a maximum of 500 genes. Higher O/E indicates more possibility of target sites.

Similar to the other databases, DIANA-microT (<http://diana.imis.athena-innovation.gr>) was put with ‘hsa-miR-372-3p’ as an initial input. The scoring system considers various features such as sequence complementarity, local structural accessibility, and conservation. Higher scores indicate more reliable and significant miRNA-target interactions. The results will be ranked by miTG score system which is determined by considering the combined weights of all miRNA recognition elements (MREs), both conserved and non-conserved, located on the 3' untranslated region (UTR) of the target mRNA. A higher miTG score implies a higher precision of the predicted mRNA.

Plasmid construction

The following primers were used to amplify mature miR-372 sequence. The retrieved product size was 552 bp.

Table 3. Primers used for miR-372 cloning.

Forward with EcoRI restriction site	GCT GAATTC ACTTGCGATCGCCGCCTTG
Reverse with BamHI restriction site	CGAG GATCC AGCCGCCCTCTGAACCTTC

Enzyme digestion

PCR products obtained from PCR were digested using the following reagents listed in the table below. The reactions were incubated at 55°C for 2 hours.

Table 4. PCR product digestion reagents.

PCR product digestion reagents	
PCR product	25 μ l
10X rCutsmart buffer	4 μ l
BamHI - HF	1 μ l
EcoRI - HF	1 μ l
dH ₂ O	9 μ l
Total	40 μ l

pLVX-EF1 α -IRES-Puro vector was digested using the following reagents listed in the table below. The reaction was incubated at 55°C for 2 hours.

Table 5. pLVX-EF1 α -IRES-Puro digestion reagents.

pLVX-EF1 α -IRES-Puro digestion reagents	
600 ng of pLVX-EF1 α -IRES-Puro vector	
10X rCutsmart buffer	2 μ l
BamHI - HF	0.5 μ l
EcoRI - HF	0.5 μ l
dH ₂ O	
Total	20 μ l

Ligation

The table below provides the reagents used in ligation of pLVX-EF1 α -IRES-Puro backbone and PCR product. The reaction was set at room temperature overnight.

Table 6. pLVX-Ef α -IRES-Puro and PCR products ligation reagents.

pLVX-EF1 α -IRES-Puro and PCR products ligation reagents	
Digested PCR product	0.5 μ l
Digested pLVX-EF1 α -IRES-Puro	0.5 μ l
10X ligase buffer	0.5 μ l
T4 DNA ligase	0.5 μ l
dH ₂ O	3 μ l
Total	5 μ l

Gel electrophoresis

Agarose 1% gel was prepared from 1 g agarose (Vivantis, Malaysia) in 100 ml 1x Tris-acetate-EDTA (TAE) buffer before adding 5 μ l Redsafe. DNA was mixed with 6x loading glycerol buffer in ratio of 5:1. Additional TAE was used as a buffer. Gel electrophoresis was operated at 100 V of voltage for 40 minutes after loading DNA sample into the sample well.

Transformation

Forty-five μ l competent Stbl3 *E. coli* cells were added to 5 μ l of pre-chilled ligation reaction before incubating on ice for 10 minutes. The mixture was then heat shocked at 42°C for 30 seconds and incubated on ice for the next 10 minutes. To finalize the volume to 200 μ l, SOC growth media was added to the mixture followed by incubating at 37°C and shaking at 800 rpm for 40 minutes.

Two hundred μ l of *E. coli* cells were plated onto pre-warmed LB/ampicillin plate and incubated at 37°C overnight.

Positive colony selection PCR

Isolated colony was selected for PCR. The table below provides the reagents used in this process. The primers for detection were listed (5' -3'): forward: GGC AGG GAT ATT CAC CAT TAT CG; reverse GAA TAC TGC CAT TTG TCT CGA GG.

Table 7. Colony selection PCR reagents.

Colony selection PCR reagents (1 reaction)	
10X reaction buffer	1.25 µl
MgCl ₂	0.375 µl
dNTP	0.25 µl
Forward primer	0.25 µl
Reverse primer	0.25 µl
Taq DNA polymerase (Biotech rabbit)	0.05 µl
dH ₂ O	10.125 µl
Total	12.5 µl

A selected colony was inoculated in 50 µl Luria Broth (LB) media/ampicillin. The same colony was also inoculated in prepared master mix before underwent thermocycling process (Bio-Rad) using the following parameters described in the table below.

Table 8. Time and temperature used in colony selection PCR.

Time and temperature used in colony selection PCR		
Step	Temperature	Time
1	95°C	2 minutes
2	95°C	30 seconds
3	50°C	15 seconds
4	68°C	30 seconds
5	72°C	5 minutes
Repeat step 2-4 for 35 cycles		

Then, the product retrieved from PCR was subjected to gel electrophoresis. Any colony that showed the size of product match to the expected size would be chosen for further propagation. Forty μl of LB media containing selected colony was transferred to 10 ml LB media/ampicillin in 50 ml tube and incubated at 37°C overnight at 200 rpm.

Plasmid extraction and purification

Bacteria culture was extracted and purified using ZymoPURE™ Plasmid Miniprep Kit. Centrifugation of 4.5 ml of bacterial culture in 1.5 ml microcentrifuge tube was operated at full speed for 1 minute and the remaining supernatant was discarded. Pellet was resuspended by 250 μl of ZymoPURE™ P1 (Red) before adding 250 μl of ZymoPURE™ P2 (Green). The tube with the two mixtures of ZymoPURE™ and pellet was then immediately inverted for 8-10 times and incubated for 3 minutes at room temperature. Following the addition of 250 μl of ZymoPURE™ P3 (Yellow), the tube was inverted for 5 times or until the sample turns thoroughly yellow. The tube was subjected to the centrifugation at max speed prior to the transfer of 600 μl of centrifuged lysate to a new clean 1.5 ml microcentrifuge tube. Addition of 260 μl of ZymoPURE™ Binding Buffer to the lysate was done before resuspending for 15 seconds using vortex. Zymo-Spin™ II-PX Column was placed in a collection tube. All the mixture was transferred to the Zymo-Spin™ II-PX Column/Collection Tube and sit at room temperature for 1 minute before the centrifugation at max speed for 1 minute, any remaining flow through was discarded. Addition of 800 μl of ZymoPURE™ Wash 1 to the column was proceeded prior to the centrifugation at max speed and discarding the flow through, respectively. Eight hundred μl of ZymoPURE™ Wash 2 was next subjected to proceeded with the exact same procedure as ZymoPURE™ Wash 1. Before the centrifugation at max speed for 1 minute and discarding of flow through, 200 μl of ZymoPURE™ Wash 2 was added to the column. The column was further centrifuged for 3 minutes at max speed to dry any remaining residual wash buffer. The column was placed in a new 1.5 ml microcentrifuge tube and prewarmed

25 μl ZymoPURE™ Elution Buffer at 50°C was directly added to the column. After the incubation of 10 minutes at room temperature, the column/tube was centrifuged for 1 minute and the flow-through was collected, respectively.

Transfection

HEK293FT cell culture in 6-well plate at 90% confluence were transfected using Lipofectamine™ 3000 Transfection Reagent (Invitrogen™). Two clean 1.5 ml microcentrifuge tubes were labeled as tube A and tube B, respectively. Tube A comprised of 250 μl Opti-MEM I Reduced Serum Medium and 7 μl Lipofectamine 3000 Transfection Reagent. Tube B contained 250 μl Opti-MEM I Reduced Serum Medium, 6 μl P3000 Enhancer Reagent, 2 μg psPAX2 (BX), and 1.4 μg pVSVg (VG). The mixture in tube A was transferred to tube B and incubated at room temperature for 15 minutes. Meanwhile, 990 μl media in HEK293FT culture was removed before adding 500 μl of the mixture in dropwise manner. Following the incubation of cell culture for 6 hours at 37°C with 5% CO₂, the existing media was removed and replaced by 2 ml of high-glucose Dulbecco's modified eagle medium (DMEM) supplemented with 10% fetal bovine serum, 2 mM L-glutamine, and antibiotics (100 U ml⁻¹ penicillin, 100 μg ml⁻¹ streptomycin). An additional 1 ml of media was added in the following day.

Cell culture

HepG2 (ATCC) has been derived from 15-year-old Caucasian male without the infection of HBV or HCV. SNU-449 (ATCC) is a human HCC cell line isolated from HCC tissue grade II-III/IV of 52-year-old male. Both HepG2 and SNU-449 exhibit an epithelial-like morphology. However, unlike HepG2, SNU-449 features a trace of HBV. JHH-4 (Japanese Collection of Research Bioresources Cell Bank), an HCC cell line isolated from HCC tissue of 51-year-old male, features none of HBV or HCV.

HepG2 was cultured in low-glucose Dulbecco's modified eagle medium (DMEM) supplemented with 10% fetal bovine serum, 2 mM L-glutamine, and antibiotics (100 U ml⁻¹ penicillin, 100 μg ml⁻¹ streptomycin). JHH-4 cell line was cultured in Eagle's

minimum essential media (EMEM) whereas SNU-449 cell line was cultured in Roswell Park Memorial Institute (RPMI) 1640 medium, and both cell lines used the same supplements as in HepG2 culture. All cells were maintained at 37°C with 5% CO₂.

MiRNA extraction and reverse transcription

HepG2, JHH-4, and SNU-449 cell lines were subjected to miRNA extraction using GenUP™ Micro RNA kit (Biotechrabbit). Firstly, 400 µl lysis Buffer LYSIS LR was added to the culture and sit at room temperature for 2 minutes before transferring to a Mini Filter DNA (blue) in a Collection Tube. The filter/collection tube was centrifuged at max speed for 1 minute and the filter was discarded. Following the addition of 400 µl isopropanol to the filtrate, the mixture was transferred to the Mini Filter RNA (Violet) placed in a new Collection tube before centrifugation at max speed for 2 minutes. The filtrate was discarded prior to the addition of 500 µl Buffer Wash A and the centrifugation at max speed for 1 minute, respectively. Again, the filtrate was discarded. Seven hundred µl Buffer WASH B was then subjected through the exact procedure as Buffer WASH A. The filter/collection tube was centrifuged at max speed for 3 minutes to dry ethanol residuals before discarding the collection tube. Following the transfer of Mini Filter RNA (Violet) to an Elution Tube, 30 µl RNase-free water was added directly to the column. Lastly, the column was incubated at room temperature for 1 minute before the centrifugation at max speed for 1 minute.

Retrieved miRNA was polyuridylated using the reagents listed in the table below before incubated at 37°C for 10 minutes. The mastermix was then added by 0.4 µl of 10 µM SL-PolyA prior to the incubation at 65°C for 5 minutes and on ice for 2 minutes, respectively.

Table 9. MiRNA polyuridylation reagents

miRNA polyuridylation reagents	
10X NEBuffer (NEB)	2.5 μ l
50 mM UTP (Thermofisher)	0.25 μ l
40 U/ μ l Ribolock (Thermofisher)	1 μ l
2 U/ μ l PoluU polymerase (NEB)	1 μ l
500 ng miRNA	
Distilled water	
Total	25 μ l

The reaction was incubated at 37°C for 10 minutes before the addition of 0.4 μ l of 10 μ M SL-PolyA. Next, the reaction was then incubated at 65°C for 5 minutes followed by incubation on ice for 2 minutes. The reagents listed in the table below were added to reverse miRNA and the reaction was incubated at 42°C for 60 minutes, and 70° for 10 minutes, respectively.

Table 10. MiRNA reverse transcription reagents.

miRNA reverse transcription reagents	
5X RT (NEB)	8 μ l
10 mM dNTPs (Thermofisher)	4 μ l
200 U RevertAid (Thermofisher)	2 μ l
40 U/ μ l Ribolock	1 μ l
Total	15 μ l

MRNA extraction and reverse transcription

Total RNA purification kit (NorgenBiotek) was used to extract and purify RNA extracted from HepG2, JHH-4, and SNU-449 cell lines cultured in 24-well plate. First, cell medium was removed and 400 μ l of Buffer RL was added to the well. After the incubation for 1 minute, cell lysate was transferred to the blue column before subjected to max speed centrifugation at room temperature. Blue column was discarded following the centrifugation, and the flow-through was then thoroughly mix

with 400 μ l 70% ethanol. Next, the solution was transferred to the red column, followed by the max speed centrifugation at room temperature. The flow-through was discarded before the addition of 500 μ l Wash Buffer and max speed centrifugation for 1 minute, respectively. After discarding the flow-through, washing the column with 500 μ l Wash Buffer was repeated for additional 2 times. The column was centrifuged for 3 minutes to dry the remaining wash buffer. The column was transferred to 1.5 ml microcentrifuge tube and 30 μ l Nuclease free water was added directly to the column. The column was incubated at room temperature for 1 minute prior to the max speed centrifugation.

Retrieved mRNA was subjected to reverse transcription to generate cDNA using the reagents listed in the table below.

Table 11. CDNA synthesis reagents.

cDNA synthesis reagents	
iScript™ Reverse Transcriptase 5x	4 μ l
RNA	600 ng
Distilled water	
Total	20 μ l

The reaction was placed in the thermocycler (Bio-Rad) set with the parameters described in the table below. Working cDNA template can be generated by adding 80 μ l distilled water to the reaction once completed the thermocycling process.

Table 12. Time and temperature used mRNA reverse transcription.

Time and temperature used mRNA reverse transcription		
Step	Temperature	Time
1	25°C	5 minutes
2	46°C	45 minutes
3	95°C	1 minute

Quantitative Real time-polymerase chain reaction (qRT-PCR)

Reversed mRNA or miRNA was mixed with reactions listed in the table below.

Table 13. qRT-PCR reagents.

qRT-PCR reagents	
4x CAPITAL™ qPCR Probe Master Mix (Biotech Rabbit)	2.5 µl
10 µM/µl forward primer	0.25 µl
10 µM/µl reverse primer	0.25 µl
Distilled water	6 µl
cDNA template	1 µl
Total	10 µl

MiRNA expression was quantified by QuantStudio3 (Thermofisher) with the following parameters described in the table below. Primers for qRT-PCR were listed (5'-3'): U6 forward: CTC GCT TCG GCA GCA CAG; miR-372-3p forward: AGT GCT GCG ACA TTT GAG CG; universal reverse: GCA GGG TCC GAG GTA TTC.

Table 14. Time and temperature used in miRNA qRT-PCR.

Time and temperature used in miRNA qRT-PCR		
Step	Temperature	Time
1	95°C	10 minutes
2	95°C	15 seconds
3	55°C	15 seconds
4	72°C	20 seconds
Repeat step 2-4 for 45 cycles		

mRNA expression was quantified by QuantStudio3 (Thermo Fisher).

Table 15. Time and temperature used in mRNA qRT-PCR.

Time and temperature used in mRNA qRT-PCR		
Step	Temperature	Time
1	50°C	2 minutes
2	95°C	10 minutes
3	60°C	1 minute
Repeat step 2-3 for 40 cycles		

Table 16. Primers for qRT-PCR

Primer	Sequence (5'-3')	Concentration
RPL19 forward	GCT CTT TCC TTT CGC TGC T	10 μ M/ μ l
RPL19 reverse	CAT TGG TCT CAT TGG GGT CT	
CDK2 forward	GCA TCT TTG CTG AGA TGG TGA CT	
CDK2 reverse	TCA TCC AGG GGA GGT ACA ACT T	
CCND1 forward	GAC CCC GCA CGA TTT CAT TG	
CCND1 reverse	AAT GAA CTT CAC ATC TGT GGC AC	
CCND2 forward	CTG TGT GCC ACC GAC TTT AAG	
CCND2 reverse	GAC AAT CCA CGT CTG TGT TGG	
E2F1 forward	CCA GGA AAA GGT GTG AAA TCC C	
E2F1 reverse	CGT TGG TGA TGT CAT AGA TGC G	
E2F2 forward	ACA AGA GGC TGG CCT ATG TGA	
E2F2 reverse	GCA GGT TGT CCT CAG TCC TGT	
E2F3 forward	CCT GAC TCA ATA GAG AGC CTA CA	
E2F3 reverse	CCA AGT CTT TGG AAG CGG G	
E2F5 forward	GAT CTC AAA GCG GCT GCT GAT A	
E2F5 reverse	CAG CAC CTA CAC CTT TCC ACT G	
CDC25A forward	CAA GGA AAA TGA AGC CTT TGA GTT	
CDC25A reverse	TGA GGA AAG CAT CCG AGC T	

Dual luciferase reporter assay

HEK293FT cells were seeded into 96-well plate in concentration of 1×10^4 cells per well. pmirGLO and pSilencer 3.0-H1 vector were used in this experiment. pmirGLO vector contains firefly luciferase and renilla luciferase gene, and pSilencer employs RNA polymerase III promotor, allowing inserted miRNA sequence to be transcribed. Firstly, pmirGLO was digested by XhoI and SacI and ligated to wild-type or mutant 3'UTR of target gene, respectively. The sequence of miR-372-3p was digested using BamHI and HindIII and was ligated to pSilencer 3.0-H1 vector. All the vectors were introduced to HEK293FT cell line using jetPRIME® transfection reagent according to the manufacturer's protocol. Luciferase activity measurement was carried out using Dual-Luciferase® Reporter Assay kit with minor modifications. After 24 hours of transfection, the cells were lysed with 20 μ l 1X passive lysis buffer (PLB). The culture was placed on shaker for 15 minutes at room temperature before adding 50 μ l LAR II into each well. Firefly luciferase activity can now be detected using Synergy™ HTX multi-mode reader (Thermo Fisher Scientific). Next, 50 μ l Stop & Glo® reagent was poured into each well to cease firefly luciferase activity. Finally, renilla luciferase activity was measured using the same equipment.

Cell proliferation assay

MTT assay

Cells were seeded into 96-well plate in concentration of 5×10^3 cells per well. MTT (3-(4,5-dimethylthazol-2-yl)-2,5-diphenyl tetrazolium bromide) (Sigma-Aldrich) was prepared in final concentration of 0.5 mg/ml in low glucose DMEM without FBS and streptomycin and penicillin. Cells were incubated at 37°C with 5% CO₂ for 30 minutes. Once incubated, media was removed and replaced by 100 μ l dimethyl sulfoxide (DMSO)(Sigma-Aldrich), respectively. The culture was then incubated at 37°C with 5% CO₂ for 5 minutes and was kept from the exposure of light.

The absorbance of each well was analyzed by BioTek™ Synergy™ HTX Multi-mode Microplate Reader (Thermo Fisher Scientific) using wavelength of 570 nm.

BrdU assay

To prepare 10 mM BrdU stock solution, 100 mg BrdU was dissolved in 32.5 ml DMSO. Next, BrdU stock solution was diluted in cell culture medium with ratio 1:1000 to make 10 μ M BrdU labeling solution. Blocking buffer was prepared by dissolving 5% BSA in permeabilization buffer. Cells were seeded into 24-well plate in concentration of 1×10^5 cells/ml and were incubated for 48 hours without perturbation prior to the assay. Cell medium was replaced by 500 μ l 10 μ M BrdU labeling solution, and cells were incubated at 37°C with 5% CO₂ overnight. The labeling solution was removed, and the cells were washed with PBS 3 times with 2 minutes each.

After removing the PBS, 500 μ l 4% formaldehyde in PBS was added to the culture. Cells were incubated at 37°C with 5% CO₂ for 15 minutes before washing with PBS 3 times with 2 minutes each. Followed by the removal of PBS, 500 μ l Triton X-100 permeabilization buffer was then added. Cells were incubated for 20 minutes at room temperature prior to the removal of Triton X-100 permeabilization buffer and replacing with 500 μ l 2N HCl, respectively. Cells were incubated at room temperature for 30 minutes. After the removal of 2N HCl, washing with Triton X-100 permeabilization buffer 3 times with 2 minutes each was then proceeded. Next, 500 μ l blocking buffer was added to the culture and the cells were incubated at room temperature for 30 minutes.

Blocking buffer was removed and 500 μ l of blocking buffer with anti-BrdU primary antibody (sc-32323; Santa Cruz) in 1:200 ratio was added to the culture. After the incubation at room temperature overnight, cells

were washed with Triton X-100 permeabilization buffer 3 times with 5 minutes each. Secondary antibody (1:500 dilution) and DAPI (1:1000 dilution) were added to the culture and the cells were incubated at room temperature for 1 hour. Washing with Triton X-100 permeabilization buffer 3 times with 5 minutes each was then proceeded before the addition of PBS to the culture. The cells were observed under the fluorescence microscope.

Cell counting

Cells were counted using ImageJ program, and EVOS™ FL Auto 2 Imaging System was used to take 10 random microscopic fields of each well, including more than 10,000 nuclei in total. Each field was processed into 8-bit scale and was later adjusted the threshold. The field was converted to binary before using Watershed option to separate cell boundaries from each other. Finally, Analyze particles option was used to count all the cells in the field.

Protein extraction

Cells were lysed with 0.25% trypsin for 3 minutes, and the cell lysate was neutralized and transferred to 1.5 ml microcentrifuge tube, respectively. Next, the cell lysate was spun down with 130 rcf for 2 minutes. Supernatant was then removed and 200 µl 1X protease inhibitor in RIPA buffer was mixed and resuspended with cell lysate in 1.5 ml microcentrifuge tube, respectively. The protein lysates were kept at -80°C until use.

Bradford assay

Standard BSA (1 mg/ml) was mixed with DI water at different dilutions, such as 0, 0.2, 0.4, 0.8, and 1 mg/ml, for standardization. Ten µl of each BSA dilution was poured into separate microtiter plate wells with its duplicate. Dye was prepared in ratio 1:5 and was added to each microtiter plate wells in volume of 200 µl. The microtiter plate was incubated at room temperature for 5 minutes before proceeding to absorbance measurement by BioTek™ Synergy™ HTX Multi-mode Microplate

Reader (Thermo Fisher Scientific) using wavelength of 595 nm. The absorbance of protein was subtracted by the absorbance of standard at 0 mg/ml and was subjected to protein concentration (X) calculation using equation: $(8.1919(X)) - 0.479$. Next, 5X Laemmli was mixed with protein to make the final calculated concentration before boiling at 100°C for 5 minutes.

SDS-PAGE gel electrophoresis (Western Blot)

12% resolving gel solution was made by mixing 2.8 ml DI water, 1.5 ml 40% acrylamide/Bis, 628 μ l 1.5 M Tris-HCl pH 8.8, 50 μ l 10% SDS, 37.3 μ l 10% APS, and 2.67 μ l TEMED. The resolving gel solution was loaded in between glass plate and short plate. 1 ml DI water, 154 μ l 40% acrylamide/Bis, 400 μ l 0.5 M Tris-HCl pH 6.8, 16 μ l 10% SDS, 20 μ l 10% APS, and 2 μ l TEMED were mixed to make 3.75% stacking gel solution. The stacking gel solution was then loaded in between glass plate and short plate over the resolving gel solution before inserting gel comb. The combined plate with gel was transferred to the tank poured with 1X running buffer. The proteins were loaded separately into each well, and the voltage of 70V was used for 15 minutes before changing the voltage to 130V for 80 minutes using PowerPac™ Basic Power Supply (Bio-Rad, Hercules, California). The protein on the gel was transferred to nitrocellulose membrane at voltage of 20V for 30 minutes using PowerPac™ HC High Current Power Supply (Bio-Rad, Hercules, California). The gel was later discarded, and the nitrocellulose membrane was incubated with BlockPRO™ 1 min (Visual protein, Taipei, Taiwan) at room temperature for 2 hours on shaker. A specific primary antibody was added to the blocking buffer in ratio 1:1,000 and was incubated overnight at 4°C on shaker. The nitrocellulose was washed three times with 0.05% tween in 1X TBST (10 minutes each). BlockPRO™ 1 min with secondary antibody in ratio 1:5,000 was used to incubate the nitrocellulose for 1 minute at room temperature on shaker. The nitrocellulose was then washed three times with 0.05% tween in 1X TBST (10 minutes each). ECL detection reagents (Amersham™,

Cytiva, Massachusetts, USA) were poured over the nitrocellulose to enhance visual under UVP ChemStudio (Analytik Jena, Germany).

Statistical analysis

Data analysis from qRT-PCR and cell proliferation was performed by Graphpad Prism software version 5.00.288 (San Diego, CA, USA). The differences with p-value < 0.05, p-value < 0.01, and p-value < 0.001 were considered significant.



Results

Web-based Bioinformatic Tools Revealed the Possible Interaction between MiR-372-3p and Cell Cycle-related Target MRNAs.

A total of 16 candidate genes were selected from literature review of Otto T, and Sicinski P. Selected genes cover major five biological functions in driving cell cycle to S phase (67). CDK2, CDK4, CDK6, CCND1, CCND2, CCND3, and CCNE1 are categorized as direct regulators (67). E2F1, E2F2, E2F3, E2F4, E2F5, and E2F8 are classified as transcriptional regulators (67). CDC25A acts as a cell cycle-checkpoint, whereas PCNA and RB play an important role in DNA replication and cell proliferation suppressor, respectively (67). Four web-based bioinformatic tools were utilized to retrieve the possible interactions between miR-372-3p and cell cycle-related target mRNAs. TargetScan predicted the interaction of miR-372-3p with CDK2, CCND1, CCND2, E2F1, E2F2, E2F3, E2F5, and CDC25A, accounting for 50% of total candidate genes. miRTarBase only discovered the interaction with CDK2, and CCND2, and thus accounted for 12% of total candidate genes. CCND1, CCND2, E2F1, E2F3, and E2F5 were predicted using mirSystem, representing 31.25% of total candidate genes. DIANA-microT also predicted CCND1, E2F1, E2F2, and E2F5, and represented 25% of total candidate genes (Table 17, Figure 5).

	TargetScan	MirTarBase	mirSystem	DIANA-microT
Cyclin-dependent kinase 2 (<i>CDK2</i>)	+	+	-	-
Cyclin-dependent kinase (<i>CDK4</i>)	-	-	-	-
Cyclin-dependent kinase (<i>CDK6</i>)	-	-	-	-
Cyclin D1 (<i>CCND1</i>)	+	-	+	+
Cyclin D2 (<i>CCND2</i>)	+	+	+	-
Cyclin D3 (<i>CCND3</i>)	-	-	-	-
Cyclin E1 (<i>CCNE1</i>)	-	-	-	-
E2 factor 1 (<i>E2F1</i>)	+	-	+	+
E2 factor 2 (<i>E2F2</i>)	+	-	-	+
E2 factor 3 (<i>E2F3</i>)	+	-	+	-
E2 factor 4 (<i>E2F4</i>)	-	-	-	-
E2 factor 5 (<i>E2F5</i>)	+	-	+	+
E2 factor 8 (<i>E2F8</i>)	-	-	-	-
Cell division cycle 25 homolog A (<i>CDC25A</i>)	+	-	-	-
Proliferating cell nuclear antigen (<i>PCNA</i>)	-	-	-	-
Retinoblastoma (<i>RB</i>)	-	-	-	-

Table 17. Overall web-based bioinformatic program prediction of candidate cell cycle related genes.

A

TargetScan prediction	
Gene	Total context score
CDK2	-0.31
CCND1	-0.24
CCND2	-0.28
E2F1	-0.17
E2F2	-0.29
E2F3	-0.03
E2F5	-0.35
CDC25A	-0.09

B

miRTarBase data collection		
Gene	Sum of evidence	Number of paper
CDK2	3	2
CCND1	-	-
CCND2	2	2
E2F1	-	-
E2F2	-	-
E2F3	-	-
E2F5	-	-
CDC25A	-	-

C

miRSystem prediction	
Gene	O/E ratio
CDK2	-
CCND1	2.97071
CCND2	1.90349
E2F1	4.70199
E2F2	-
E2F3	2.04023
E2F5	6.45453
CDC25A	-

D

DIANA micro-T prediction	
Gene	miTG score
CDK2	-
CCND1	0.785444
CCND2	-
E2F1	0.816729
E2F2	0.773375
E2F3	-
E2F5	0.984714
CDC25A	-

Figure 5. Prediction of cell cycle-related gene and miR-372-3p from each web-based bioinformatic program. (A) TargetScan. (B) miRTarBase. (C) miRSystem. (D) DIANA micro-T.

Decreased MiR-372-3p Expression Was Found in HCC Cell Line.

The qPCR analysis was used to investigate the nature of miR-372-3p expression in different HCC cell lines and normal hepatocyte cell line, THLE-2. The results indicated that JHH-4 and HepG2 had a significant lower miR-372-3p expression compared to THLE-2 (Figure 6).

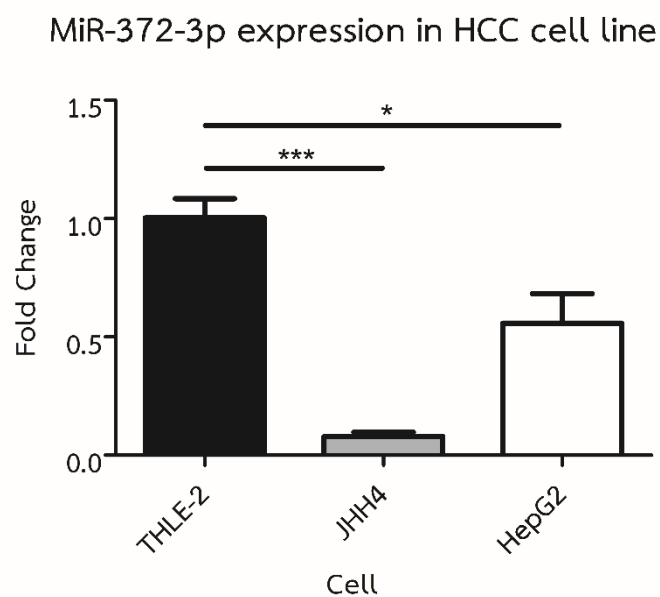


Figure 6. MiR-372-3p expression in THLE-2, JHH-4, and HepG2 cell line. Data are shown as mean \pm SD and expressed relative to those of control (set as 1.0). $N \geq 3$ replicates per group from at least two independent experiments. Student's t-test; * = $p < 0.05$, *** = $p < 0.001$.

PCR Product Verification

The products retrieved from PCR amplification were subjected to gel electrophoresis and sequencing, respectively. The DNA ladder was in the first lane and the PCR product was in the second lane as depicted in Figure 7A. Sequencing result also confirmed the successful ligation of PCR product and LVX-EF1 α vector. MiR-372 sequence was located at 295 bp to 362 bp (Figure 7B).

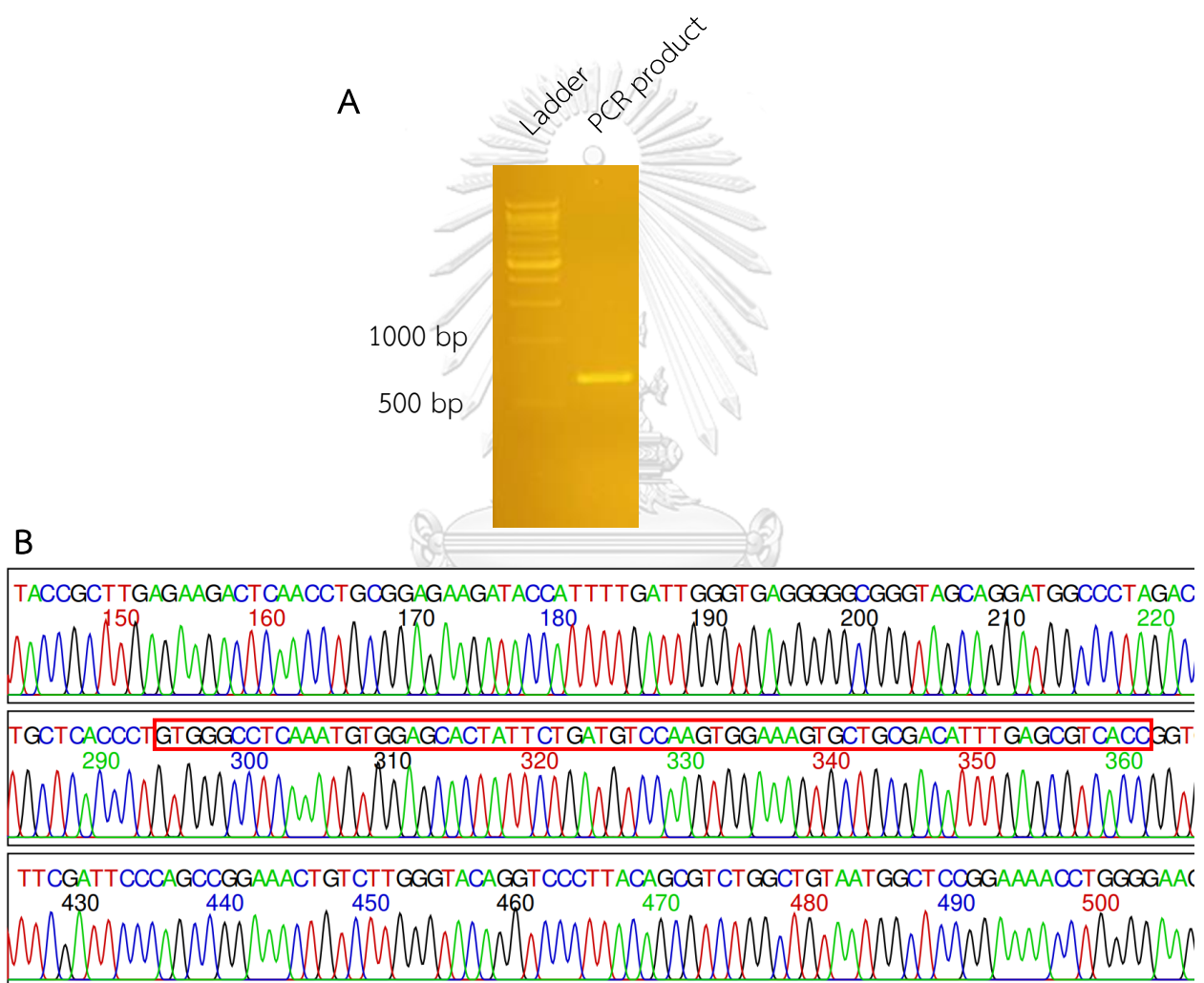


Figure 7. Verification of constructed LVX-EF1a-miR-372 vector. **(A)** Gel electrophoresis of amplified PCR miR-372 sequence. **(B)** Sanger sequencing of constructed vector indicated miR-372 sequence at 295 bp to 362 bp (labeled in red rectangular box).

Selection of Established HCC Cell Lines

Transduced HepG2 and negative control were treated with 1 mg/ml puromycin whereas JHH-4 cell line and negative control were treated with 2 mg/ml puromycin. SNU-449 cell line and negative control were treated with 5 mg/ml puromycin. Overall cell confluence of control and miR-372-3p group increased overtime. In contrast, the cell confluence of negative control, which contains no miR-372-3p overexpressing vector, gradually declined in 6 days (Figure 8-10).

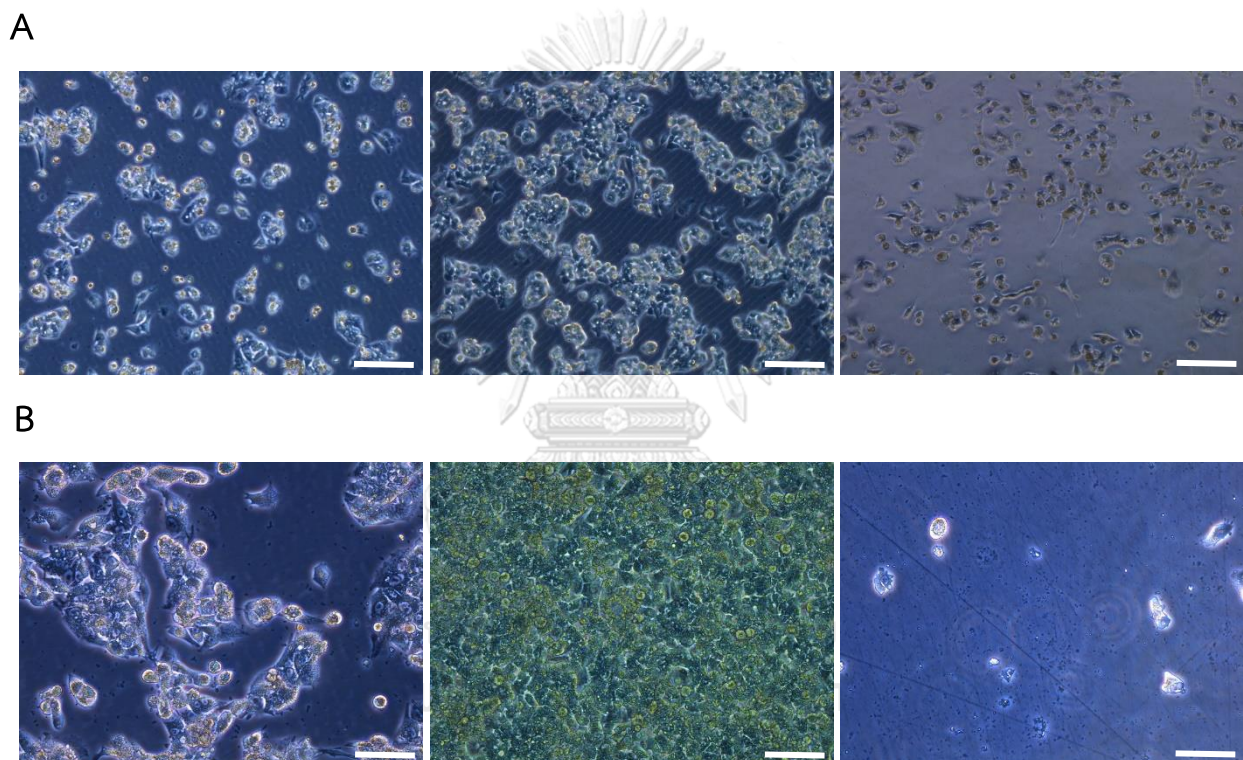
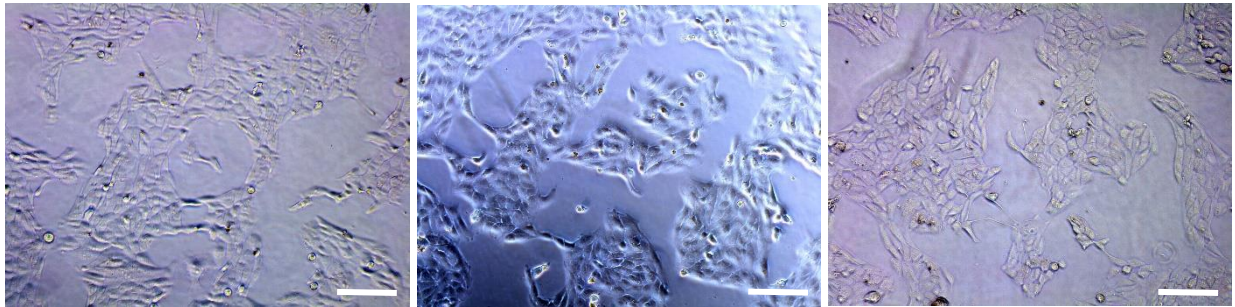


Figure 8. Puromycin selection of MiR-372-3p overexpressing HepG2. (A) Two-day post-selection. Control HepG2 (left panel). miR-372-3p overexpressing HepG2 (middle panel). Negative control (right panel). Scale bars, 100 μm (B) Six-day post-selection. Control HepG2 (left panel). miR-372-3p overexpressing HepG2 (middle panel). Negative control (right panel). Scale bars, 50 μm .

A



B

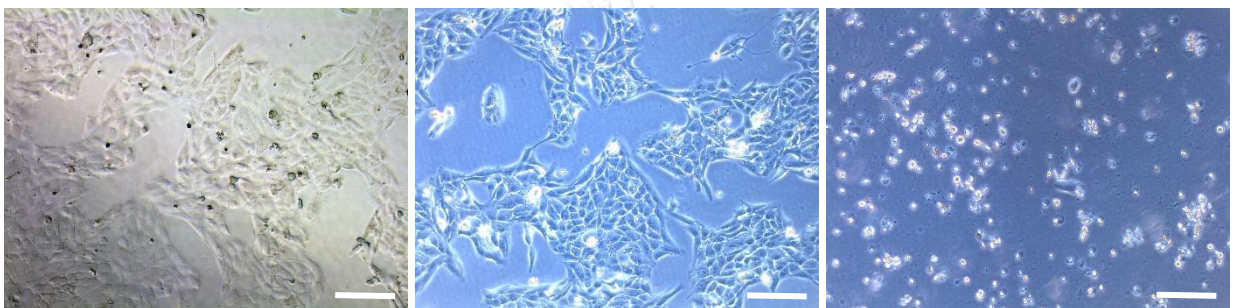
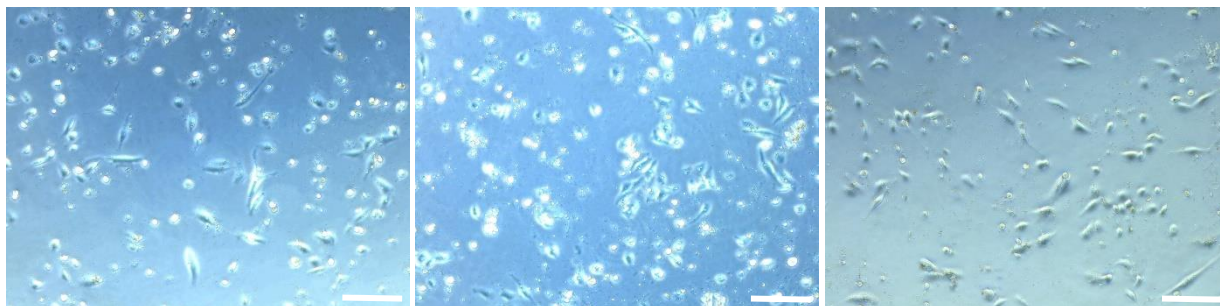


Figure 9. Puromycin selection of MiR-372-3p overexpressing JHH-4. (A) Two-day post-selection. Control JHH-4 (left panel). miR-372-3p overexpressing JHH-4 (middle panel). Negative control (right panel). (B) Six-day post-selection. Control JHH-4 (left panel). miR-372-3p overexpressing JHH-4 (middle panel). Negative control (right panel). Scale bars, 100 μ m.

A



B

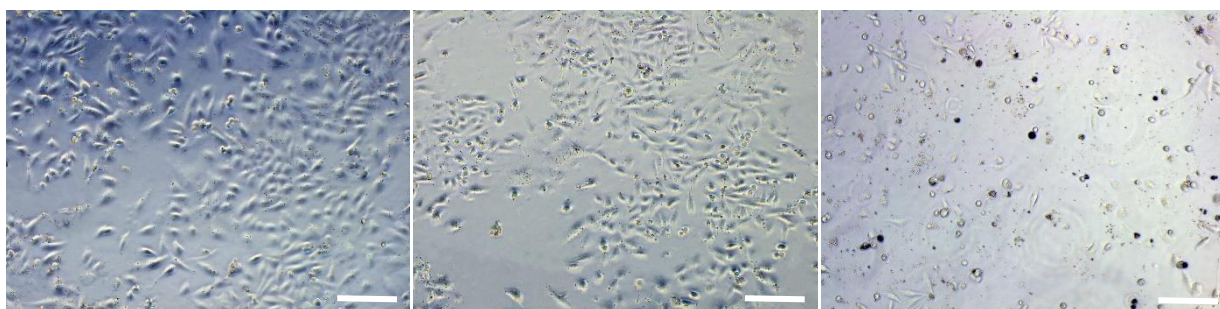


Figure 10. Puromycin selection of MiR-372-3p overexpressing SNU-449. (A) Two-day post-selection. Control SNU-449 (left panel). miR-372-3p overexpressing SNU-449 (middle panel). Negative control (right panel). (B) Six-day post-selection. Control SNU-449 (left panel). miR-372-3p overexpressing SNU-449 (middle panel). Negative control (right panel). Scale bars, 100 μm .

Transduced HCC Cell Lines Expressed a Higher Level of MiR-372-3p.

To investigate the expression of miRNA-372-3p, the established HCC cell lines were subjected to qPCR analysis. Transduced HepG2 exhibited a higher expression of miRNA-372-3p compared to wild-type. As well as in transduced JHH-4 and SNU449 cell line, both of them showed a significantly higher expression of miRNA-372-3p than their wild-type counterpart (Figure 11).

MiR-372-3p Expression in Transduced HCC Cell Lines

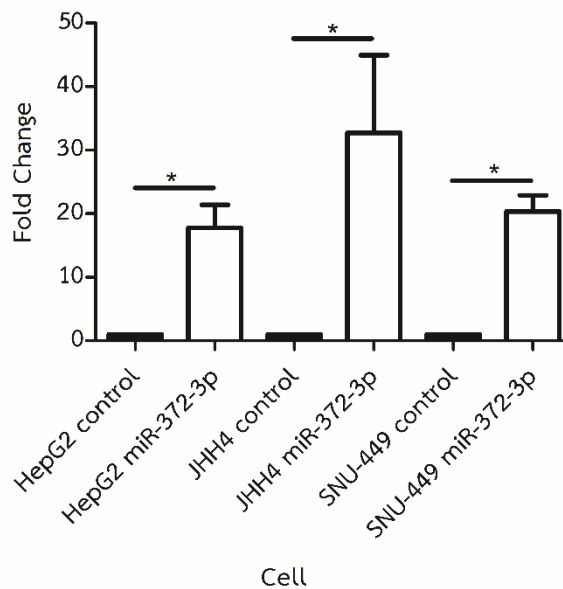


Figure 11. The expression of miR-372-3p in different transduced HCC cell lines. Data are represented as mean \pm SD and expressed relative to those of control (set as 1.0). $N > 3$ replicates per group from at least two independent experiments. Student's t-test; * = $p < 0.05$.

Changes in Cell Cycle-Related mRNA Were Detected in Established HCC Cell Line.

MRNA expression of major proteins involved with cell cycle was proceeded in different established HCC cell lines using qPCR quantification. Validated major proteins regulating cell cycle progression included CDK2, CCND1, E2F1, E2F2, and E2F3. In JHH-4, these proteins were majorly downregulated compared to control. Transduced HepG2, however, showed different results. Only CCND1 expression was downregulated, whereas CDK2, E2F1, and E2F2 possessed a higher expression and E2F3 mRNA level remained unchanged compared to control. Interestingly, transduced SNU-449 exhibited several upregulated cell cycle-related mRNA expressions such as CDK2, CCND1, CDC25A, E2F1, E2F2, and E2F3 (Figure 12).



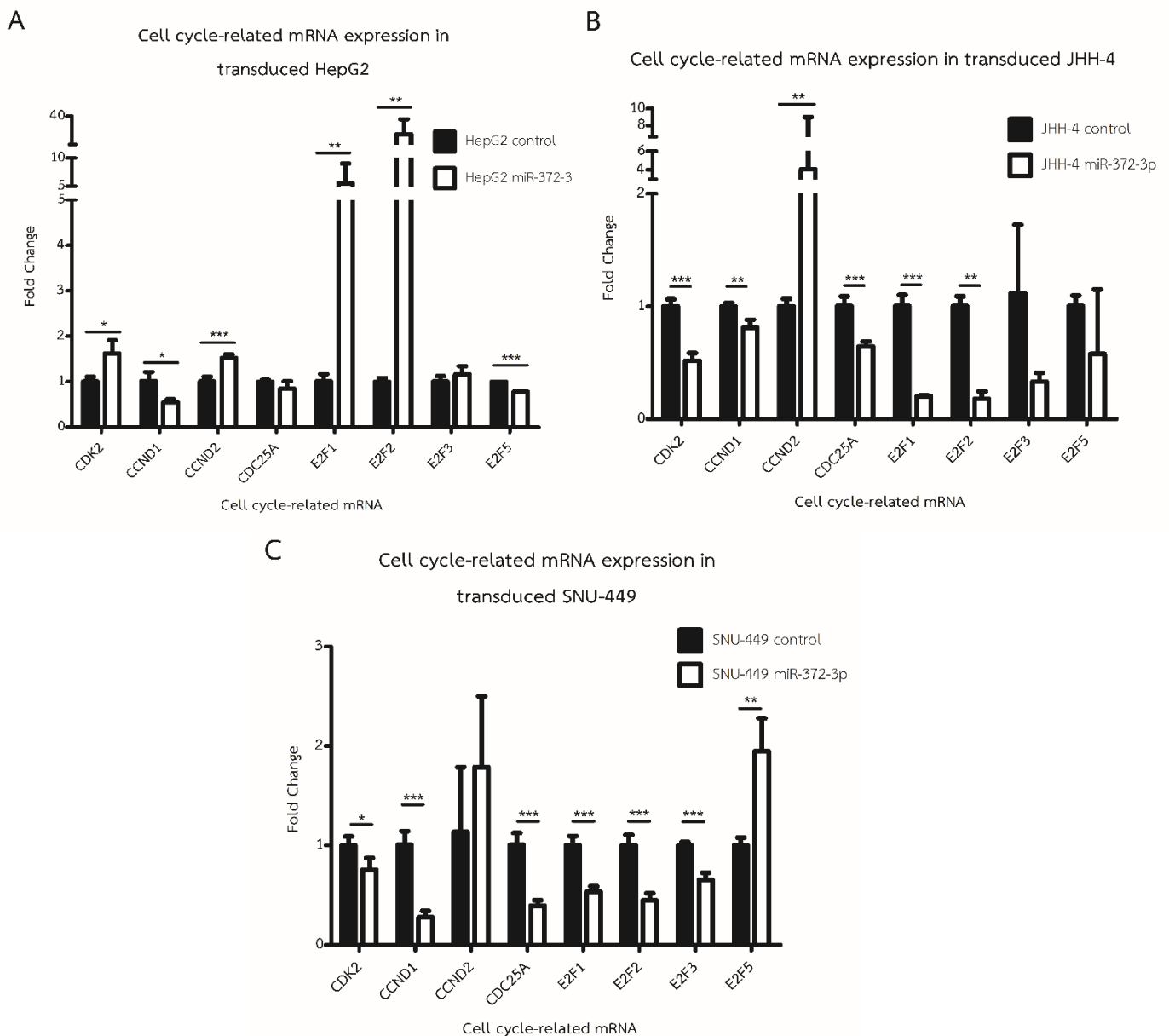


Figure 12. Cell cycle related-mRNA expression in miR-372-3p overexpressing HCC cell lines. **(A)** Expression of cell cycle-related mRNA in miR-372-3p overexpressing JHH-4. **(B)** Expression of cell cycle-related mRNA in miR-372-3p overexpressing HepG2. **(C)** Expression of cell cycle-related mRNA in miR-372-3p overexpressing SNU-449. Data are shown as mean \pm SD and expressed relative to those of control (set as 1.0). $N > 3$ replicates per group from at least two independent experiments. RPL19 was used as a housekeeping gene and internal control. Student's t-test; * $p < 0.05$; ** $p < 0.01$; *** $p < 0.001$.

MiRNA-372-3p Decreased CCND1 mRNA Expression.

According to previous qPCR data, CCND1 mRNA expression was the only mRNA that was downregulated in all transduced HCC cell lines. Luciferase assay was then used to determine the interaction between miR-372-3p and CCND1 UTR. Four different CCND1 UTR sequences were illustrated in Figure 11A. Luciferase activity of wild-type is the weakest compared to that of control. All three mutants exhibited a significantly higher relative luminescence compared to that of wild-type as showed in Figure 13B.

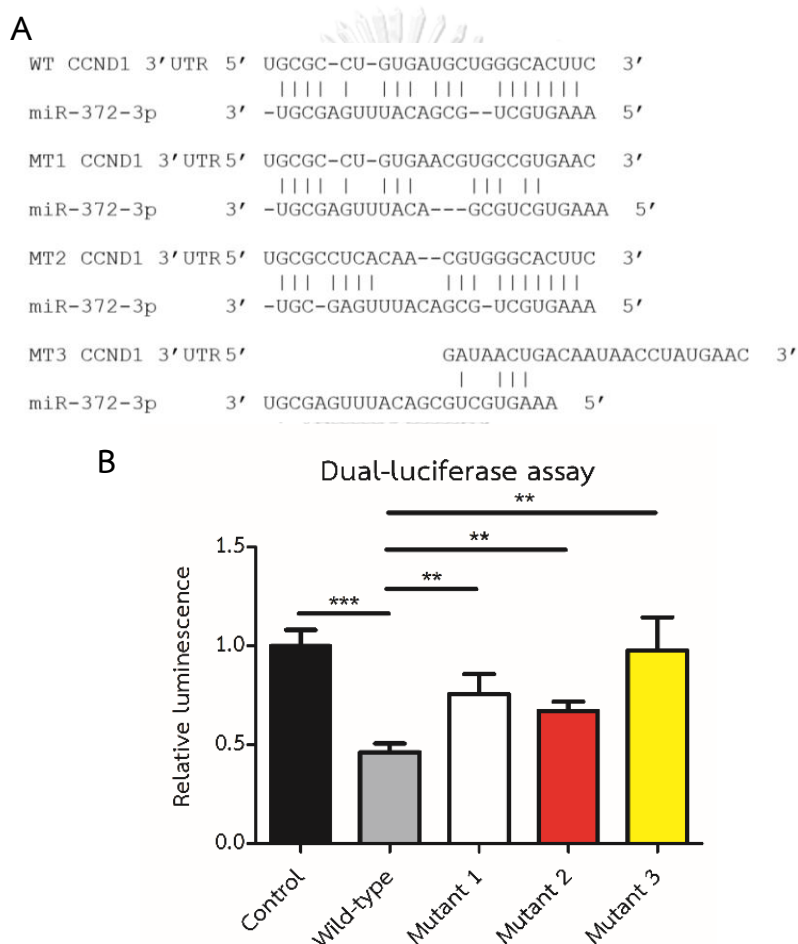


Figure 13. Dual-luciferase assay indicated that miR-372-3p targets CCND1 3'-UTR. **(A)** RNA hybridization pattern between miRNA-372-3p and wild-type (WT) 3'-UTR or three different 3'-UTR mutants (MT1-MT3). **(B)** Dual luciferase reporter assay of wild-type and mutant 1, mutant 2, and mutant 3. Data are represented as mean \pm SD. N = 3 replicates per group. Student's t-test; * = $p < 0.05$; ** = $p < 0.01$; *** = $p < 0.001$.

Deterred HCC Cell Line Proliferation as a Result of miRNA-372-3p Overexpression

MTT assay was carried out to determine the change in proliferation rate of transduced HCC cell lines. The proliferation rate of transduced HepG2 was significantly decreased compared to that of control, especially in day 2. Transduced JHH-4 began to decline their proliferation rate at day 2, and day 3. In addition, transduced SNU-449 showed a significantly lower proliferation rate since day 1 (Figure 14).

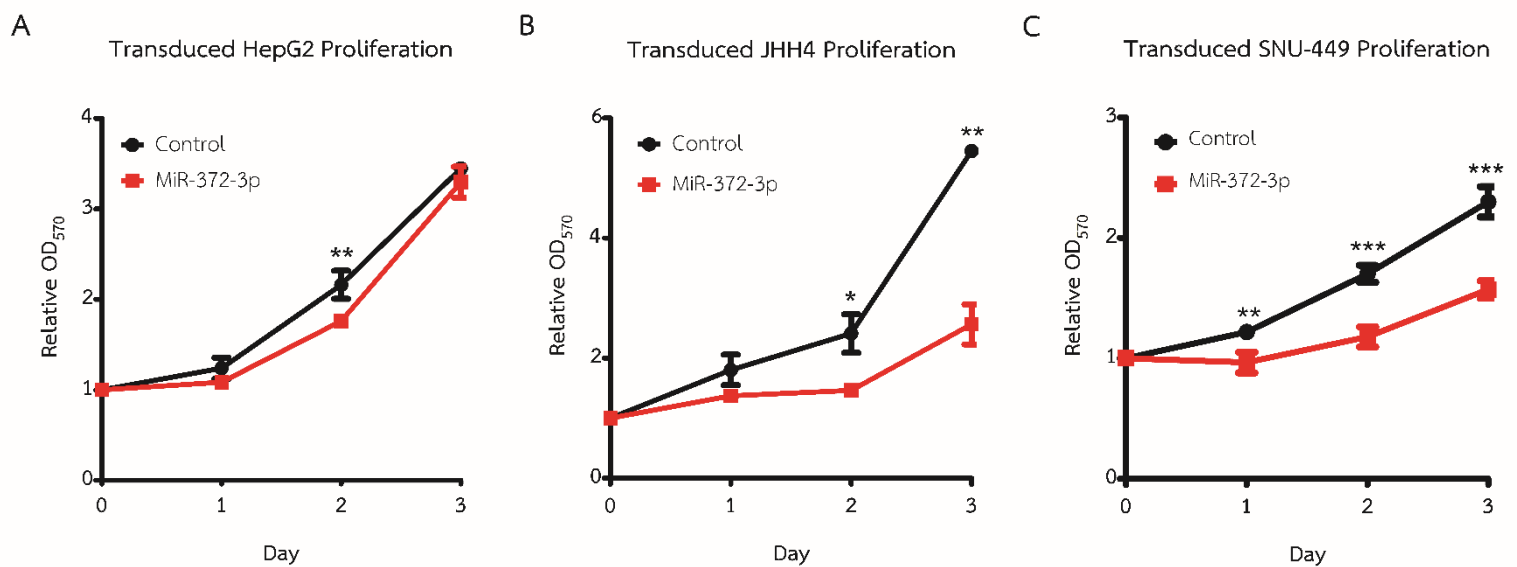
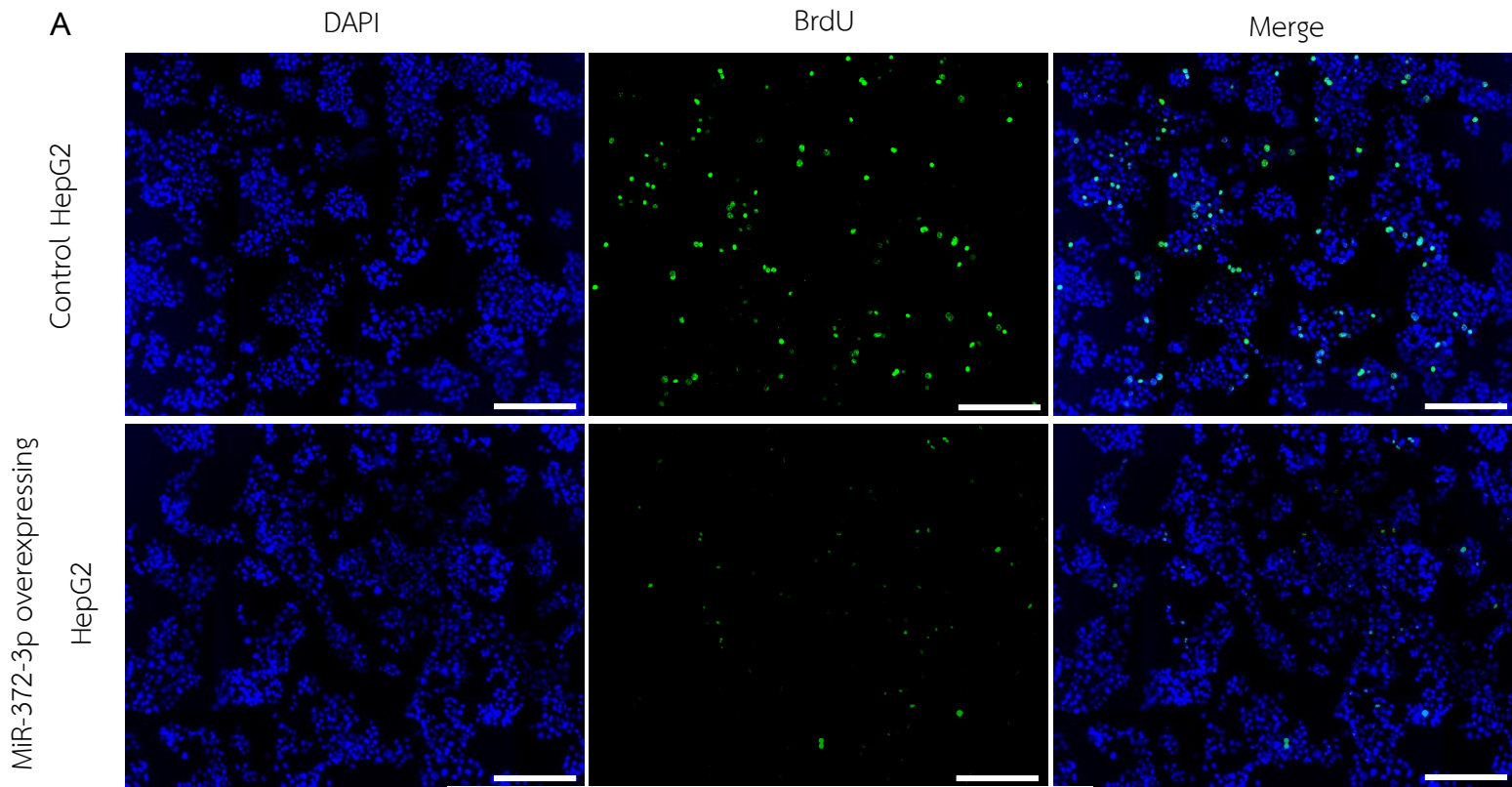


Figure 14. The proliferation rate was reduced in miR-372-3p overexpressing cell line.

(A) HepG2, (B) JHH-4, and (C) SNU-449. Data are represented as mean \pm SD and expressed relative to those of control (set as 1.0). N > 3 replicates per group.

Student's t-test; * = $p < 0.05$; ** = $p < 0.01$; *** = $p < 0.001$.

To narrow down the phase of cell cycle affected by overexpression of miR-372-3p, BrdU incorporation assay was then performed. HepG2 control showed higher BrdU positive cells (4.56%) compared to that of miR-372-3p overexpressing HepG2 (0.34%) (Figure 15). MiR-372-3p overexpressing SNU-449 also exhibited a lower BrdU positive cells (16.81%) compared to that of control SNU-449 (33.72%) (Figure 16).



B Transduced HepG2 BrdU incorporation assay

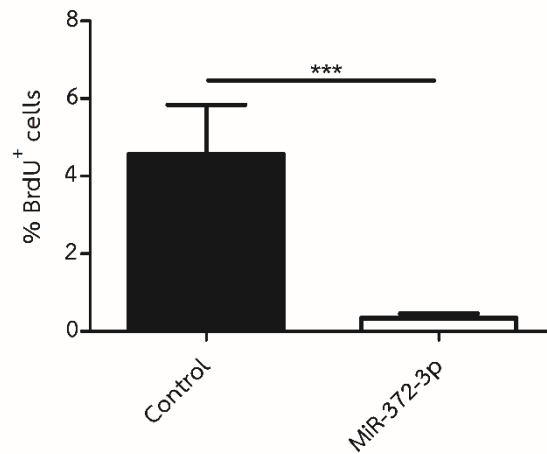
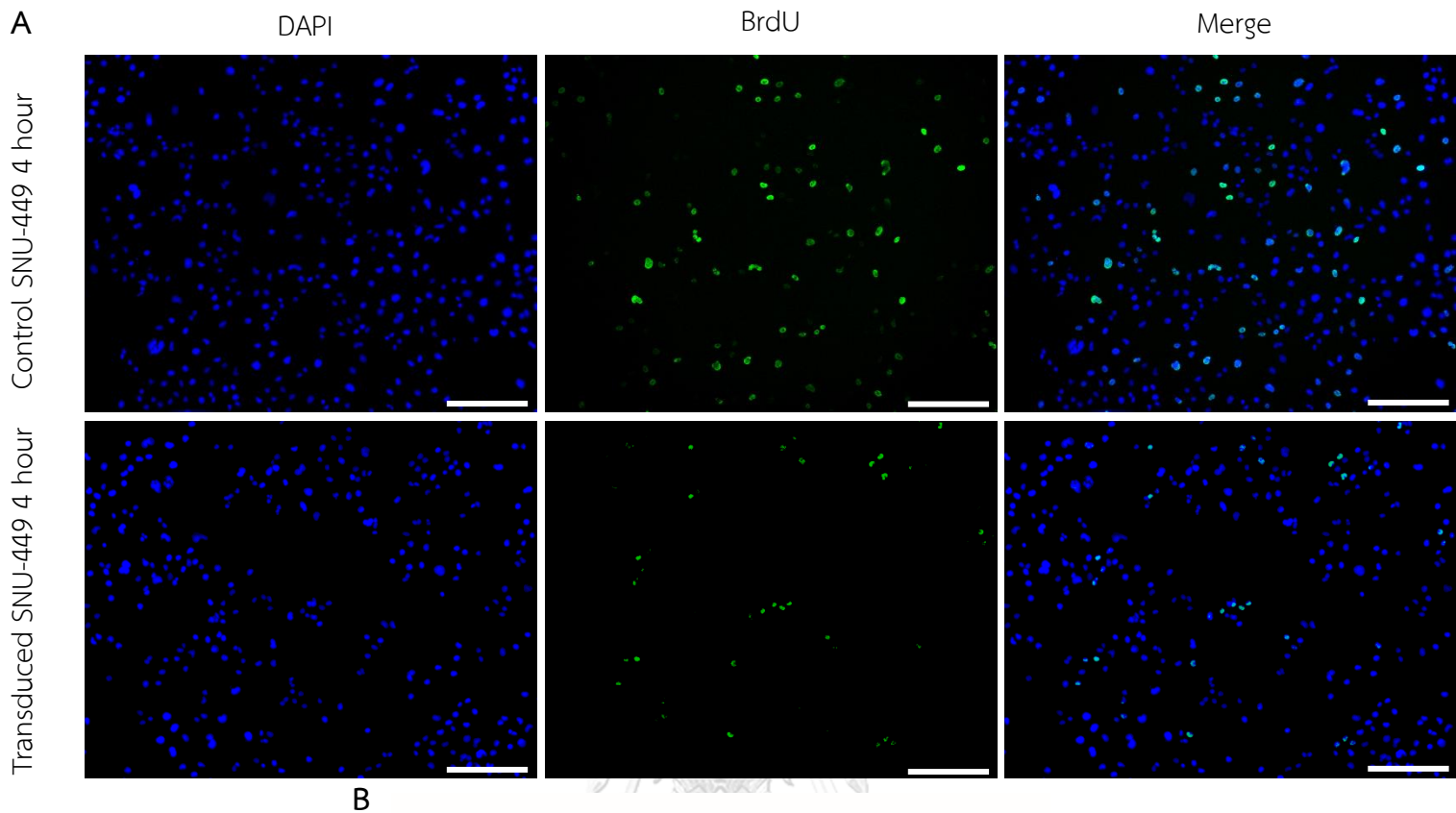


Figure 15. BrdU incorporation assay of transduced HepG2. (A) Representative fields of HepG2 are shown with DAPI (left panels), BrdU (middle panels), and merge (right panels). (B) Quantitative result of BrdU stained HepG2. Fluorescent images taken at equivalent exposure for comparison. Scale bars, 100 μ m. DAPI: 4'6-diamidino-2-phenylindole. Data are showed as mean \pm SD. *** = $p < 0.001$.



Transduced SNU-449 BrdU incorporation assay

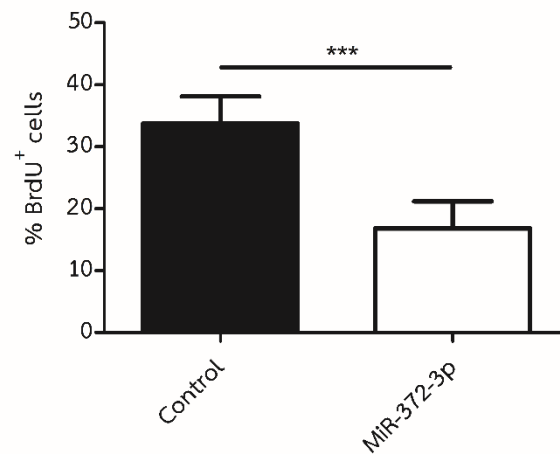


Figure 16. BrdU incorporation assay of transduced SNU-449. (A) Representative fields of SNU-449 are shown with DAPI (left panels), BrdU (middle panels), and merge (right panels). (B) Quantitative result of BrdU stained SNU-449. Fluorescent images taken at equivalent exposure for comparison. Scale bars, 100 μ m. DAPI: 4'6-diamidino-2-phenylindole. Data are showed as mean \pm SD. *** = $p < 0.001$.

Cyclin D1 Protein Expression Decreased in Transduced HCC Cell Line.

Western blot analysis revealed the decrease in cyclin D1 protein expression in transduced HepG2 cell line compared to control. However, cyclin D1 expression in transduced JHH-4 cell line showed a subtle difference compared to control (Figure 17).

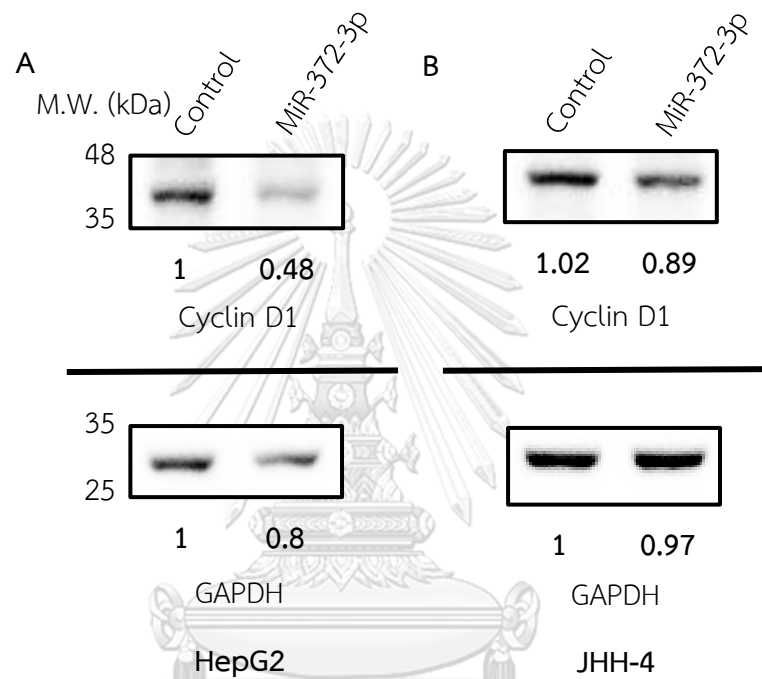


Figure 17. Western blot of miR-372-3p overexpressing HepG2 and JHH4 indicates the amount of cyclin D1.

DISCUSSION & CONCLUSION

The roles of miR-372-3p seem to vary in each type of cancer. As depicted in previous research, miR-372-3p may have an anti-oncogenic property in colon cancer cell line, but it turns into oncogenic roles in lung squamous cell carcinoma. However, their functions in HCC have been rarely explored.

First, the expression of miR-372-3p in wild-type HCC cell line was investigated. MiR-372-3p expression in normal liver cell line was relatively high than in wild-type HCC cell lines. In consistent with the findings, previous research showed that miR-372 expression in HCC tumor retrieved from patient was also relatively lower than in adjacent normal tissue (103), suggesting that miR-372 might play a crucial role in HCC progression. Although, some findings lead to the entirely opposite outcome. It was reported that miR-372 expression is relatively high in HCC tissue compared to adjacent tissue (111). Moreover, miR-372 positively correlates to a low survival rate after surgery in HCC patients (111). From G. Wu, et al. study, miR-372 expression in HCC cell lines is relatively low compared to that of control, which also correlates with the present findings (103). In contrast, the study from G. Wu, et al. showed that miR-372 expression in HCC cell lines is relatively high compared to that of control (111). However, the HCC cell lines used in these studies are LO2 (HL-7702), SMMC7721, and QGY7701, which have been considered as problematic cell lines due to contamination of HeLa (112). Therefore, the results from these studies may not be translatable to the present study. Recent study indicated that cell lines that have been established in China were mostly misidentified (85.51%) and were cross-contaminated (25%) (112). In addition, cell lines that were found contaminated in China laboratories were contaminated from HeLa or HeLa derivatives (112).

After introducing the miR-372-3p overexpression vector to HCC cell lines, the selection of established cell lines was then proceeded at different concentration of puromycin. HepG2 was treated with 1 mg/ml puromycin, whereas JHH-4 and SNU-449 were treated with 2 and 5 mg/ml puromycin, respectively. HCC cells transduced with miR-372-3p overexpression vector increased their confluence, while negative control that did not receive overexpression vector gradually decreased their confluence over

time until completely vanished within 8 days. qPCR analysis showed that all the transduced cell lines produced miR-372-3p in a higher level compared to positive control, which was introduced with vector containing red fluorescence protein sequence, mCherry, and puromycin resistance gene. Thus, the production of miR-372-3p in established cell lines was confirmed. MTT assay was carried out to measure cell proliferation. Among the three HCC cell lines, JHH-4 control seems to have much higher relative absorbance compared to that of SNU-449. This might result from the difference in doubling time of each cell line. According to the previous study, the fastest JHH-4 doubling time was 32.99 hours (113), whereas the doubling time of SNU-449 ranged from 36 to 27.74 hours (113, 114). Thus, it is possible that JHH-4 might replicate faster than SNU-449, increasing the relative absorbance. However, relative absorbance of HepG2 in day 3 was not significantly different between control and miR-372-3p overexpressing HepG2. Inconsistent cell seeding might be the cause of these indifferences.

Utilizing BrdU incorporation assay, the number of transduced HCC cells that enter S phase can be quantified. BrdU is a thymine analog and can be taken into the cells, especially during DNA replication stage, S phase. After phosphorylated, BrdU is now turned into BrdUTP which is recognized by DNA polymerase and is thus incorporated into DNA, replacing thymine. Therefore, BrdU incorporation assay is highly effective in determining the progression of cell cycle phase from G1 to S. Both miR-372-3p overexpressing HepG2 and JHH-4 showed a significantly lower BrdU positive cell in percentage compared to their control. However, the data from JHH-4 is still lacking as a result of technical difficulties. After puromycin selection of miR-372-3p overexpressing JHH-4, the cell confluence was drastically decreased compared to control, resulting in limited use in further experiments.

Both MTT and BrdU indicated the decline in proliferation rate of all transduced HCC cell lines, implying that overexpression of miR-372-3p might impede cell cycle progression, especially from G1 to S phase. These results are in accordance with the previous findings. It was reported that the upregulation of miR-372-3p could reduce cell proliferation in HepG2 and induce apoptosis (115). However, some research contradicts the obtained results. MiRNA-372 was found to induce HCC cell

proliferation via targeting ATAD2 and driving cell cycle from G1 to S phase, respectively (25). However, the latter study employed CCK8 and colony forming assay to evaluate proliferation rate, and they also used short interference RNA to ATAD2 in HCC cell lines in those experiments (25). In addition, many problematic cell lines, such as SMMC7721, QGY7721, LO2, were used to quantify ATAD2 protein expression (25). Hence, it is possible that the results they obtained may not be translatable to the present study because of the indirect inhibition of mRNA target rather than miRNA itself and the use of problematic cell lines.

According to previous researches, major cell cycle regulators involving the transition from G1 to S phase have been well-depicted such as, CDK2/4/6, CCND1/2/3, CCNE1, E2F1/2/3/4/5/8, CDC25A, PCNA, and RB (116-124). These cell cycle related genes were thus chosen for target screening using web-based bioinformatic programs: TargetScan, miRTarBase, miRSystem, and DIANA-microT. The prediction indicates that miR-372-3p may hold a potential to interfere with only some of them. Among four web-based tools, TargetScan could predict the most target mRNA including CCND1, CCND2, CDC25A, CDK2, E2F1, E2F2, and E2F3. Thus, investigating these mRNA expressions in miR-372-3p overexpressing HCC cell lines is essential.

Quantification of major cell-cycle related mRNAs regulating G1 to S phase in established HCC cell lines was then proceeded. The results indicated that each HCC cell line had a different gene expression. According to the previous study, overexpression of miR-372 in nasopharyngeal carcinoma cell line showed that CDK2, and TP53 expression were downregulated (125). Another study in cervical cancer cell line, CDK2 was negatively correlated to miR-372 expression (126). Decreased CDK2 expression was found in miR-372-3p overexpressing JHH-4 and SNU-449 in the present study. However, lower expression of TP53 allows CDK2 and cyclin E to initiate the progression of cell cycle to S phase (127). From the study in HUH7, miR-372 also reduced the expression of E2F1 and thus interfered cell proliferation, respectively (128). A similar outcome was found in miR-372-3p overexpressing JHH-4 and SNU-449 due to the significantly lower expression of E2F1 compared to control. There is evidence reported that E2F5 expression was highly abundant in wild-type HepG2, and repressing it by short interference RNA led to a reduction in cell number entering S

phase (129). Upregulated E2F5 in HepG2 control confirms the correlation to the previous study. A specific gene can be expressed differently among cell lines, depending on the type and nature of each cell line. For instance, a high level of p21 in wild-type HepG2 induces the expression of cyclin E (130). In contrast, wild-type JHH-4 and HUH7 with p21 expression appear normal cyclin E level (130). This could be used to explain the difference in cell cycle-related mRNA expressions in three different HCC cell lines. However, most of the conducted study used HepG2, one of the most popular HCC models, while the other models such as JHH-4, and SNU-449 are still left uninvestigated.

Dual-luciferase assay was then employed to test whether 3'-UTR of CCND1 is a target of miR-372-3p. Low relative luminescence in wild-type group compared to control or mutant group suggested that miR-372-3p could bind to 3'-UTR of CCND1. Finally, western blot was later carried out to quantify CCND1 protein level in miR-372-3p overexpressing HCC cell lines. Cyclin D1 expression in miR-372-3p overexpressing HepG2 is obviously lower than in control. In the other way, miR-372-3p overexpressing JHH-4 seems to have less obvious difference of cyclin D1 expression between the group. Note that the measurement of cyclin D1 protein level in SNU-449 is still lacking due to technical difficulties, and two more independent repeats of HepG2 and JHH-4 would be sufficient for statistical analysis and protein level quantification. However, future study should explore more of G1-S phase cell cycle-related protein expressions other than cyclin D1 since some of mRNA expressions may not always positively correlate to its protein expression (131). Several factors have been known to cause this inconsistency. Post-transcriptional modifications such as alternative splicing, and stability of mRNA could alter protein expression (132). Thus, it is plausible that some protein that were originally downregulated or upregulated in mRNA level might increase or decrease its expression in protein level.

This study faces some limitations. Despite two independent experiments in measuring the mRNA expression, all the samples were from the same biological sample. Thus, it is suggested that the experiment should be repeated with whole different biological samples. In addition, subjecting miR-372-3p overexpressing HCC

cells to RNA sequencing would reveal new downregulated biological pathways or targets for further study.

To conclude, miR-372-3p may hold a dramatic effect to HCC cell lines when overexpressed. The presence of miR-372-3p may interfere with the translation of CCND1 mRNA in HepG2 cell line by binding to 3'-UTR of CCND1 mRNA, interfering the entering to S phase of cell cycle (Figure 18). The findings of this study address the function of miR-372-3p and its effects on the proliferation of HCC cell lines that are involved with cell cycle regulation. All results obtained from this study might be applicable to HCC therapeutic options in the future.

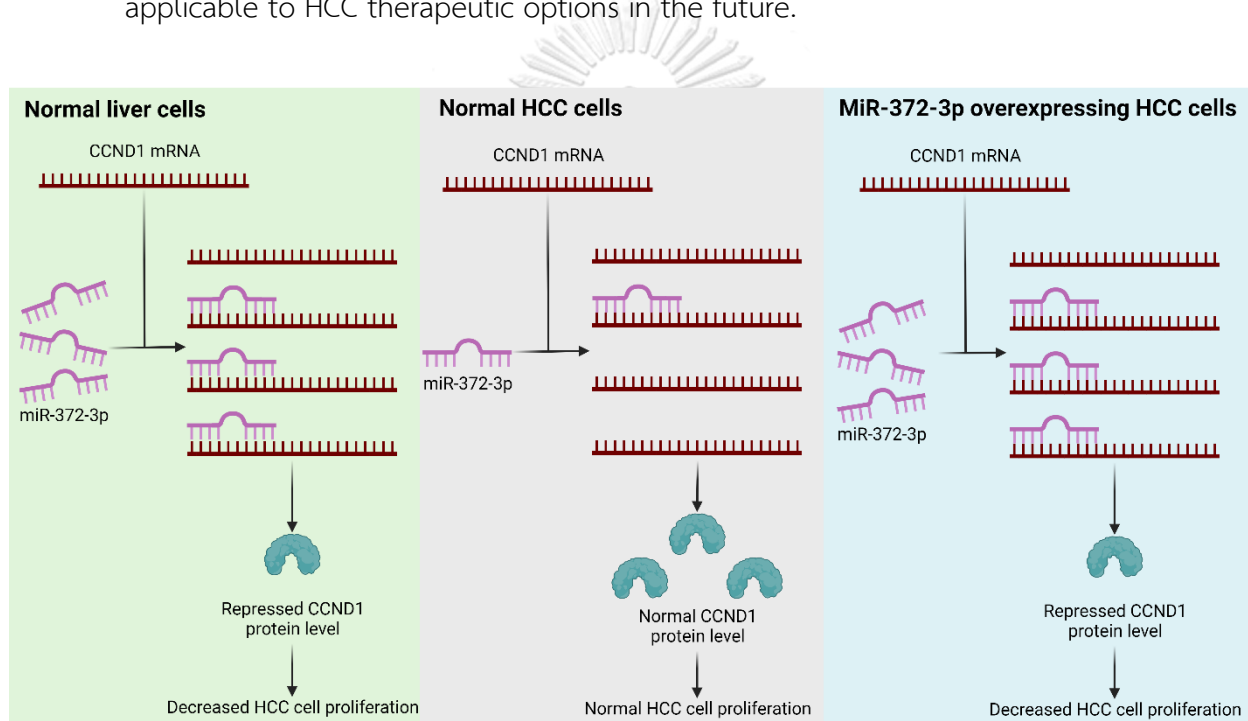


Figure 18. Proposed mechanism of miR-372-3p/CCND1 in HCC cells. Low level of miR-372-3p in normal HCC allows the translation of CCND1 mRNA and drives the cell cycle transition from G1 to S, respectively. In miR-372-3p overexpressing HCC cells, the translation of CCND1 becomes interfered due to high level of miR-372-3p, thus tampering cell cycle progression.

REFERENCES

1. CDC. Hepatocellular carcinoma - United States, 2001-2006. *MMWR Morb Mortal Wkly Rep.* 2010;59(17):517-20.
2. Yang JD, Hainaut P, Gores GJ, Amadou A, Plymoth A, Roberts LR. A global view of hepatocellular carcinoma: trends, risk, prevention and management. *Nat Rev Gastroenterol Hepatol.* 2019;16(10):589-604.
3. Balogh J, Victor D, 3rd, Asham EH, Burroughs SG, Boktour M, Saharia A, et al. Hepatocellular carcinoma: a review. *J Hepatocell Carcinoma.* 2016;3:41-53.
4. Llovet JM, Zucman-Rossi J, Pikarsky E, Sangro B, Schwartz M, Sherman M, et al. Hepatocellular carcinoma. *Nature Reviews Disease Primers.* 2016;2(1):16018.
5. Hanahan D, Weinberg RA. Hallmarks of cancer: the next generation. *Cell.* 2011;144(5):646-74.
6. Fry DW, Harvey PJ, Keller PR, Elliott WL, Meade M, Trachet E, et al. Specific inhibition of cyclin-dependent kinase 4/6 by PD 0332991 and associated antitumor activity in human tumor xenografts. *Mol Cancer Ther.* 2004;3(11):1427-38.
7. Szabo G, Bala S. MicroRNAs in liver disease. *Nat Rev Gastroenterol Hepatol.* 2013;10(9):542-52.
8. Dharap A, Pokrzywa C, Murali S, Pandi G, Vemuganti R. MicroRNA miR-324-3p induces promoter-mediated expression of RelA gene. *PLoS One.* 2013;8(11):e79467.
9. Huntzinger E, Izaurralde E. Gene silencing by microRNAs: contributions of translational repression and mRNA decay. *Nat Rev Genet.* 2011;12(2):99-110.
10. Abd ElAziz ON, Elfiky AM, Yassin MA, Abd El-Hakam FE, Saleh EM, El-Hefnawi M, et al. In Silico and In Vivo Evaluation of microRNA-181c-5p's Role in Hepatocellular Carcinoma. *Genes (Basel).* 2022;13(12).
11. Ding J, Huang S, Wu S, Zhao Y, Liang L, Yan M, et al. Gain of miR-151 on chromosome 8q24.3 facilitates tumour cell migration and spreading through downregulating RhoGDIA. *Nat Cell Biol.* 2010;12(4):390-9.
12. Tan W, Li Z, Xia W, Zhu J, Fan R. miR-221-3p regulates hepatocellular carcinoma cell proliferation, migration and invasion via targeting LIFR. *Ann Hepatol.* 2022;27 Suppl

1:100567.

13. Zhang W, Qian S, Yang G, Zhu L, Zhou B, Wang J, et al. MicroRNA-199 suppresses cell proliferation, migration and invasion by downregulating RGS17 in hepatocellular carcinoma. *Gene*. 2018;659:22-8.
14. Zhang NS, Dai GL, Liu SJ. MicroRNA-29 family functions as a tumor suppressor by targeting RPS15A and regulating cell cycle in hepatocellular carcinoma. *Int J Clin Exp Pathol*. 2017;10(7):8031-42.
15. Wang Y, Sun B, Sun H, Zhao X, Wang X, Zhao N, et al. Regulation of proliferation, angiogenesis and apoptosis in hepatocellular carcinoma by miR-26b-5p. *Tumour Biol*. 2016;37(8):10965-79.
16. Shi L, Zhang J, Pan T, Zhou J, Gong W, Liu N, et al. MiR-125b is critical for the suppression of human U251 glioma stem cell proliferation. *Brain Res*. 2010;1312:120-6.
17. Huang L, Luo J, Cai Q, Pan Q, Zeng H, Guo Z, et al. MicroRNA-125b suppresses the development of bladder cancer by targeting E2F3. *Int J Cancer*. 2011;128(8):1758-69.
18. Butz H, Likó I, Czirják S, Igaz P, Khan MM, Zivkovic V, et al. Down-regulation of Wee1 kinase by a specific subset of microRNA in human sporadic pituitary adenomas. *J Clin Endocrinol Metab*. 2010;95(10):E181-91.
19. Friedman SL. Liver fibrosis -- from bench to bedside. *J Hepatol*. 2003;38 Suppl 1:S38-53.
20. Friedman SL. Hepatic stellate cells: protean, multifunctional, and enigmatic cells of the liver. *Physiol Rev*. 2008;88(1):125-72.
21. Coll M, El Taghdouini A, Perea L, Mannaerts I, Vila-Casadesús M, Blaya D, et al. Integrative miRNA and Gene Expression Profiling Analysis of Human Quiescent Hepatic Stellate Cells. *Sci Rep*. 2015;5:11549.
22. Yin G, Yan C, Hao J, Zhang C, Wang P, Zhao C, et al. PRDM16, negatively regulated by miR-372-3p, suppresses cell proliferation and invasion in prostate cancer. *Andrologia*. 2022:e14529.
23. Li Y, Li F, Feng C, Wu T, Chen Y, Shah JA, et al. MiR-372-3p Functions as a Tumor Suppressor in Colon Cancer by Targeting MAP3K2. *Front Genet*. 2022;13:836256.
24. Peng H, Pan X, Su Q, Zhu LS, Ma GD. MiR-372-3p promotes tumor progression

- by targeting LATS2 in colorectal cancer. *Eur Rev Med Pharmacol Sci.* 2019;23(19):8332-44.
25. Wu G, Liu H, He H, Wang Y, Lu X, Yu Y, et al. miR-372 down-regulates the oncogene ATAD2 to influence hepatocellular carcinoma proliferation and metastasis. *BMC Cancer.* 2014;14:107.
26. Tang A, Hallouch O, Chernyak V, Kamaya A, Sirlin CB. Epidemiology of hepatocellular carcinoma: target population for surveillance and diagnosis. *Abdom Radiol (NY).* 2018;43(1):13-25.
27. Network CGAR. Comprehensive and Integrative Genomic Characterization of Hepatocellular Carcinoma. *Cell.* 2017;169(7):1327-41.e23.
28. Paterlini-Bréchet P, Saigo K, Murakami Y, Chami M, Gozuacik D, Mugnier C, et al. Hepatitis B virus-related insertional mutagenesis occurs frequently in human liver cancers and recurrently targets human telomerase gene. *Oncogene.* 2003;22(25):3911-6.
29. Calderaro J, Couchy G, Imbeaud S, Amaddeo G, Letouzé E, Blanc JF, et al. Histological subtypes of hepatocellular carcinoma are related to gene mutations and molecular tumour classification. *J Hepatol.* 2017;67(4):727-38.
30. Chiang DY, Villanueva A, Hoshida Y, Peix J, Newell P, Minguez B, et al. Focal gains of VEGFA and molecular classification of hepatocellular carcinoma. *Cancer Res.* 2008;68(16):6779-88.
31. Stender S, Loomba R. PNPLA3 Genotype and Risk of Liver and All-Cause Mortality. *Hepatology.* 2020;71(3):777-9.
32. El-Serag HB. Epidemiology of viral hepatitis and hepatocellular carcinoma. *Gastroenterology.* 2012;142(6):1264-73.e1.
33. Yang JD, Roberts LR. Hepatocellular carcinoma: A global view. *Nat Rev Gastroenterol Hepatol.* 2010;7(8):448-58.
34. Park JW, Chen M, Colombo M, Roberts LR, Schwartz M, Chen PJ, et al. Global patterns of hepatocellular carcinoma management from diagnosis to death: the BRIDGE Study. *Liver Int.* 2015;35(9):2155-66.
35. Yang JD, Gyedu A, Afihene MY, Duduyemi BM, Micah E, Kingham TP, et al. Hepatocellular Carcinoma Occurs at an Earlier Age in Africans, Particularly in Association With Chronic Hepatitis B. *Am J Gastroenterol.* 2015;110(11):1629-31.

36. Crissien AM, Frenette C. Current management of hepatocellular carcinoma. *Gastroenterol Hepatol (N Y)*. 2014;10(3):153-61.
37. D'Souza S, Lau KC, Coffin CS, Patel TR. Molecular mechanisms of viral hepatitis induced hepatocellular carcinoma. *World J Gastroenterol*. 2020;26(38):5759-83.
38. Seeger C, Mason WS. Hepatitis B virus biology. *Microbiol Mol Biol Rev*. 2000;64(1):51-68.
39. Ivanov AV, Valuev-Elliston VT, Tyurina DA, Ivanova ON, Kochetkov SN, Bartosch B, et al. Oxidative stress, a trigger of hepatitis C and B virus-induced liver carcinogenesis. *Oncotarget*. 2017;8(3):3895-932.
40. Hsieh YH, Su IJ, Wang HC, Chang WW, Lei HY, Lai MD, et al. Pre-S mutant surface antigens in chronic hepatitis B virus infection induce oxidative stress and DNA damage. *Carcinogenesis*. 2004;25(10):2023-32.
41. Kim CW, Chang KM. Hepatitis C virus: virology and life cycle. *Clin Mol Hepatol*. 2013;19(1):17-25.
42. Zheng Y, Gao B, Ye L, Kong L, Jing W, Yang X, et al. Hepatitis C virus non-structural protein NS4B can modulate an unfolded protein response. *J Microbiol*. 2005;43(6):529-36.
43. Cheng D, Zhang L, Yang G, Zhao L, Peng F, Tian Y, et al. Hepatitis C virus NS5A drives a PTEN-PI3K/Akt feedback loop to support cell survival. *Liver Int*. 2015;35(6):1682-91.
44. Zur Hausen H. The search for infectious causes of human cancers: where and why. *Virology*. 2009;392(1):1-10.
45. Kao JH, Chen PJ, Lai MY, Chen DS. Basal core promoter mutations of hepatitis B virus increase the risk of hepatocellular carcinoma in hepatitis B carriers. *Gastroenterology*. 2003;124(2):327-34.
46. Kanwal F, Kramer JR, Ilyas J, Duan Z, El-Serag HB. HCV genotype 3 is associated with an increased risk of cirrhosis and hepatocellular cancer in a national sample of U.S. Veterans with HCV. *Hepatology*. 2014;60(1):98-105.
47. Burt AD, Lackner C, Tiniakos DG. Diagnosis and Assessment of NAFLD: Definitions and Histopathological Classification. *Semin Liver Dis*. 2015;35(3):207-20.
48. Anstee QM, Reeves HL, Kotsiliti E, Govaere O, Heikenwalder M. From NASH to

HCC: current concepts and future challenges. *Nat Rev Gastroenterol Hepatol*. 2019;16(7):411-28.

49. Rosenfeld RG. Insulin-like growth factors and the basis of growth. *N Engl J Med*. 2003;349(23):2184-6.

50. Li X, Wang X, Gao P. Diabetes Mellitus and Risk of Hepatocellular Carcinoma. *Biomed Res Int*. 2017;2017:5202684.

51. Paradis V, Perlemuter G, Bonvoust F, Dargere D, Parfait B, Vidaud M, et al. High glucose and hyperinsulinemia stimulate connective tissue growth factor expression: a potential mechanism involved in progression to fibrosis in nonalcoholic steatohepatitis. *Hepatology*. 2001;34(4 Pt 1):738-44.

52. Ford ES, Cogswell ME. Diabetes and serum ferritin concentration among U.S. adults. *Diabetes Care*. 1999;22(12):1978-83.

53. Kar M, Chakraborti AS. Release of iron from haemoglobin--a possible source of free radicals in diabetes mellitus. *Indian J Exp Biol*. 1999;37(2):190-2.

54. Wang Z. Regulation of Cell Cycle Progression by Growth Factor-Induced Cell Signaling. *Cells*. 2021;10(12).

55. Panagopoulos A, Altmeyer M. The Hammer and the Dance of Cell Cycle Control. *Trends Biochem Sci*. 2021;46(4):301-14.

56. Davis PK, Ho A, Dowdy SF. Biological methods for cell-cycle synchronization of mammalian cells. *Biotechniques*. 2001;30(6):1322-6, 8, 30-1.

57. Polyak K, Kato JY, Solomon MJ, Sherr CJ, Massague J, Roberts JM, et al. p27Kip1, a cyclin-Cdk inhibitor, links transforming growth factor-beta and contact inhibition to cell cycle arrest. *Genes Dev*. 1994;8(1):9-22.

58. Schafer KA. The cell cycle: a review. *Vet Pathol*. 1998;35(6):461-78.

59. Sherr CJ, Roberts JM. CDK inhibitors: positive and negative regulators of G1-phase progression. *Genes Dev*. 1999;13(12):1501-12.

60. Lundberg AS, Weinberg RA. Functional inactivation of the retinoblastoma protein requires sequential modification by at least two distinct cyclin-cdk complexes. *Mol Cell Biol*. 1998;18(2):753-61.

61. Arroyo M, Raychaudhuri P. Retinoblastoma-repression of E2F-dependent transcription depends on the ability of the retinoblastoma protein to interact with E2F

and is abrogated by the adenovirus E1A oncoprotein. *Nucleic Acids Res.* 1992;20(22):5947-54.

62. Petersen BO, Lukas J, Sørensen CS, Bartek J, Helin K. Phosphorylation of mammalian CDC6 by cyclin A/CDK2 regulates its subcellular localization. *Embo j.* 1999;18(2):396-410.

63. Riabowol K, Draetta G, Brizuela L, Vandre D, Beach D. The cdc2 kinase is a nuclear protein that is essential for mitosis in mammalian cells. *Cell.* 1989;57(3):393-401.

64. Hydbring P, Malumbres M, Sicinski P. Non-canonical functions of cell cycle cyclins and cyclin-dependent kinases. *Nat Rev Mol Cell Biol.* 2016;17(5):280-92.

65. Leal-Esteban LC, Fajas L. Cell cycle regulators in cancer cell metabolism. *Biochim Biophys Acta Mol Basis Dis.* 2020;1866(5):165715.

66. Liew CT, Li HM, Lo KW, Leow CK, Chan JY, Hin LY, et al. High frequency of p16INK4A gene alterations in hepatocellular carcinoma. *Oncogene.* 1999;18(3):789-95.

67. Otto T, Sicinski P. Cell cycle proteins as promising targets in cancer therapy. *Nat Rev Cancer.* 2017;17(2):93-115.

68. Lee RC, Feinbaum RL, Ambros V. The *C. elegans* heterochronic gene *lin-4* encodes small RNAs with antisense complementarity to *lin-14*. *Cell.* 1993;75(5):843-54.

69. Wang XW, Heegaard NH, Orum H. MicroRNAs in liver disease. *Gastroenterology.* 2012;142(7):1431-43.

70. Ha M, Kim VN. Regulation of microRNA biogenesis. *Nat Rev Mol Cell Biol.* 2014;15(8):509-24.

71. Yang JS, Lai EC. Alternative miRNA biogenesis pathways and the interpretation of core miRNA pathway mutants. *Mol Cell.* 2011;43(6):892-903.

72. Yang JS, Maurin T, Robine N, Rasmussen KD, Jeffrey KL, Chandwani R, et al. Conserved vertebrate mir-451 provides a platform for Dicer-independent, Ago2-mediated microRNA biogenesis. *Proc Natl Acad Sci U S A.* 2010;107(34):15163-8.

73. Xie M, Li M, Vilborg A, Lee N, Shu MD, Yartseva V, et al. Mammalian 5'-capped microRNA precursors that generate a single microRNA. *Cell.* 2013;155(7):1568-80.

74. Jonas S, Izaurralde E. Towards a molecular understanding of microRNA-mediated gene silencing. *Nat Rev Genet.* 2015;16(7):421-33.

75. Ipsaro JJ, Joshua-Tor L. From guide to target: molecular insights into eukaryotic RNA-interference machinery. *Nat Struct Mol Biol.* 2015;22(1):20-8.
76. Behm-Ansmant I, Rehwinkel J, Doerks T, Stark A, Bork P, Izaurralde E. mRNA degradation by miRNAs and GW182 requires both CCR4:NOT deadenylase and DCP1:DCP2 decapping complexes. *Genes Dev.* 2006;20(14):1885-98.
77. Fabian MR, Sonenberg N. The mechanics of miRNA-mediated gene silencing: a look under the hood of miRISC. *Nat Struct Mol Biol.* 2012;19(6):586-93.
78. Vasudevan S, Steitz JA. AU-rich-element-mediated upregulation of translation by FXR1 and Argonaute 2. *Cell.* 2007;128(6):1105-18.
79. Ørom UA, Nielsen FC, Lund AH. MicroRNA-10a binds the 5'UTR of ribosomal protein mRNAs and enhances their translation. *Mol Cell.* 2008;30(4):460-71.
80. Truesdell SS, Mortensen RD, Seo M, Schroeder JC, Lee JH, LeTonqueze O, et al. MicroRNA-mediated mRNA translation activation in quiescent cells and oocytes involves recruitment of a nuclear microRNP. *Sci Rep.* 2012;2:842.
81. O'Brien J, Hayder H, Zayed Y, Peng C. Overview of MicroRNA Biogenesis, Mechanisms of Actions, and Circulation. *Front Endocrinol (Lausanne).* 2018;9:402.
82. Keka A, Martinez Medina L, Erk S, Srivastava DP, Fernandes A, Toro R, et al. Associations of the Intellectual Disability Gene MYT1L with Helix-Loop-Helix Gene Expression, Hippocampus Volume and Hippocampus Activation During Memory Retrieval. *Neuropsychopharmacology.* 2017;42(13):2516-26.
83. Yu Z, Liu Y, Li Y, Zhang J, Peng J, Gong J, et al. miRNA-338-3p inhibits glioma cell proliferation and progression by targeting MYT1L. *Brain Res Bull.* 2022;179:1-12.
84. Sur S, Steele R, Shi X, Ray RB. miRNA-29b Inhibits Prostate Tumor Growth and Induces Apoptosis by Increasing Bim Expression. *Cells.* 2019;8(11).
85. Fujisawa Y, Matsuda K, Uehara T. Osteopontin enhances the migration of lung fibroblasts via upregulation of interleukin-6 through the extracellular signal-regulated kinase (ERK) pathway. *Biol Chem.* 2020;401(9):1071-80.
86. Cheng Q, Chen M, Wang H, Chen X, Wu H, Du Y, et al. MicroRNA-27a-3p inhibits lung and skin fibrosis of systemic sclerosis by negatively regulating SPP1. *Genomics.* 2022;114(4):110391.
87. Pan Y, Liang H, Chen W, Zhang H, Wang N, Wang F, et al. microRNA-200b and

- microRNA-200c promote colorectal cancer cell proliferation via targeting the reversion-inducing cysteine-rich protein with Kazal motifs. *RNA Biol.* 2015;12(3):276-89.
88. Javanmardi S, Aghamaali MR, Abolmaali SS, Mohammadi S, Tamaddon AM. miR-21, An Oncogenic Target miRNA for Cancer Therapy: Molecular Mechanisms and Recent Advancements in Chemo and Radio-resistance. *Curr Gene Ther.* 2017;16(6):375-89.
89. Cui R, Meng W, Sun HL, Kim T, Ye Z, Fassan M, et al. MicroRNA-224 promotes tumor progression in nonsmall cell lung cancer. *Proc Natl Acad Sci U S A.* 2015;112(31):E4288-97.
90. Wang D, Han X, Li C, Bai W. FBXL3 is regulated by miRNA-4735-3p and suppresses cell proliferation and migration in non-small cell lung cancer. *Pathol Res Pract.* 2019;215(2):358-65.
91. Zhang D, Zhou P, Wang W, Wang X, Li J, Sun X, et al. MicroRNA-616 promotes the migration, invasion and epithelial-mesenchymal transition of HCC by targeting PTEN. *Oncol Rep.* 2016;35(1):366-74.
92. Dasari VR, Kaur K, Velpula KK, Gujrati M, Fassett D, Klopfenstein JD, et al. Upregulation of PTEN in glioma cells by cord blood mesenchymal stem cells inhibits migration via downregulation of the PI3K/Akt pathway. *PLoS One.* 2010;5(4):e10350.
93. Lou Z, Gong YQ, Zhou X, Hu GH. Low expression of miR-199 in hepatocellular carcinoma contributes to tumor cell hyper-proliferation by negatively suppressing XBP1. *Oncol Lett.* 2018;16(5):6531-9.
94. Giovannini C, Fornari F, Dallo R, Gagliardi M, Nipoti E, Vasuri F, et al. MiR-199-3p replacement affects E-cadherin expression through Notch1 targeting in hepatocellular carcinoma. *Acta Histochem.* 2018;120(2):95-102.
95. Furuta M, Kozaki KI, Tanaka S, Arie S, Imoto I, Inazawa J. miR-124 and miR-203 are epigenetically silenced tumor-suppressive microRNAs in hepatocellular carcinoma. *Carcinogenesis.* 2010;31(5):766-76.
96. Lin J, Huang S, Wu S, Ding J, Zhao Y, Liang L, et al. MicroRNA-423 promotes cell growth and regulates G(1)/S transition by targeting p21Cip1/Waf1 in hepatocellular carcinoma. *Carcinogenesis.* 2011;32(11):1641-7.
97. Fornari F, Gramantieri L, Ferracin M, Veronese A, Sabbioni S, Calin GA, et al. MiR-221 controls CDKN1C/p57 and CDKN1B/p27 expression in human hepatocellular

carcinoma. *Oncogene*. 2008;27(43):5651-61.

98. Xu T, Zhu Y, Xiong Y, Ge YY, Yun JP, Zhuang SM. MicroRNA-195 suppresses tumorigenicity and regulates G1/S transition of human hepatocellular carcinoma cells. *Hepatology*. 2009;50(1):113-21.

99. Li Y, Tan W, Neo TW, Aung MO, Wasser S, Lim SG, et al. Role of the miR-106b-25 microRNA cluster in hepatocellular carcinoma. *Cancer Sci*. 2009;100(7):1234-42.

100. Bueno MJ, Malumbres M. MicroRNAs and the cell cycle. *Biochim Biophys Acta*. 2011;1812(5):592-601.

101. Zhao YX, Liu HC, Ying WY, Wang CY, Yu YJ, Sun WJ, et al. microRNA-372 inhibits proliferation and induces apoptosis in human breast cancer cells by directly targeting E2F1. *Mol Med Rep*. 2017;16(6):8069-75.

102. Li G, Zhang Z, Tu Y, Jin T, Liang H, Cui G, et al. Correlation of microRNA-372 upregulation with poor prognosis in human glioma. *Diagn Pathol*. 2013;8:1.

103. Wu G, Wang Y, Lu X, He H, Liu H, Meng X, et al. Low mir-372 expression correlates with poor prognosis and tumor metastasis in hepatocellular carcinoma. *BMC Cancer*. 2015;15:182.

104. Xu SY, Xu PF, Gao TT. MiR-372-3p inhibits the growth and metastasis of osteosarcoma cells by targeting FXRD6. *Eur Rev Med Pharmacol Sci*. 2018;22(1):62-9.

105. Cheng X, Chen J, Huang Z. miR-372 promotes breast cancer cell proliferation by directly targeting LATS2. *Exp Ther Med*. 2018;15(3):2812-7.

106. Wang Q, Liu S, Zhao X, Wang Y, Tian D, Jiang W. MiR-372-3p promotes cell growth and metastasis by targeting FGF9 in lung squamous cell carcinoma. *Cancer Med*. 2017;6(6):1323-30.

107. Lewis BP, Shih IH, Jones-Rhoades MW, Bartel DP, Burge CB. Prediction of mammalian microRNA targets. *Cell*. 2003;115(7):787-98.

108. Hsu SD, Lin FM, Wu WY, Liang C, Huang WC, Chan WL, et al. miRTarBase: a database curates experimentally validated microRNA-target interactions. *Nucleic Acids Res*. 2011;39(Database issue):D163-9.

109. Lu TP, Lee CY, Tsai MH, Chiu YC, Hsiao CK, Lai LC, et al. miRSystem: an integrated system for characterizing enriched functions and pathways of microRNA

targets. PLoS One. 2012;7(8):e42390.

110. Maragkakis M, Reczko M, Simossis VA, Alexiou P, Papadopoulos GL, Dalamagas T, et al. DIANA-microT web server: elucidating microRNA functions through target prediction. Nucleic Acids Res. 2009;37(Web Server issue):W273-6.

111. Gu H, Guo X, Zou L, Zhu H, Zhang J. Upregulation of microRNA-372 associates with tumor progression and prognosis in hepatocellular carcinoma. Mol Cell Biochem. 2013;375(1-2):23-30.

112. Ye F, Chen C, Qin J, Liu J, Zheng C. Genetic profiling reveals an alarming rate of cross-contamination among human cell lines used in China. Faseb j. 2015;29(10):4268-72.

113. Qiu Z, Li H, Zhang Z, Zhu Z, He S, Wang X, et al. A Pharmacogenomic Landscape in Human Liver Cancers. Cancer Cell. 2019;36(2):179-93.e11.

114. Park JG, Lee JH, Kang MS, Park KJ, Jeon YM, Lee HJ, et al. Characterization of cell lines established from human hepatocellular carcinoma. Int J Cancer. 1995;62(3):276-82.

115. Soliman MH, Ragheb MA, Elzayat EM, Mohamed MS, El-Ekiaby N, Abdelaziz AI, et al. MicroRNA-372-3p Predicts Response of TACE Patients Treated with Doxorubicin and Enhances Chemosensitivity in Hepatocellular Carcinoma. Anticancer Agents Med Chem. 2021;21(2):246-53.

116. Besson A, Dowdy SF, Roberts JM. CDK inhibitors: cell cycle regulators and beyond. Dev Cell. 2008;14(2):159-69.

117. Gil J, Peters G. Regulation of the INK4b-ARF-INK4a tumour suppressor locus: all for one or one for all. Nat Rev Mol Cell Biol. 2006;7(9):667-77.

118. Malumbres M, Barbacid M. Cell cycle, CDKs and cancer: a changing paradigm. Nat Rev Cancer. 2009;9(3):153-66.

119. Musgrove EA, Caldon CE, Barraclough J, Stone A, Sutherland RL. Cyclin D as a therapeutic target in cancer. Nat Rev Cancer. 2011;11(8):558-72.

120. Skaar JR, Pagano M. Control of cell growth by the SCF and APC/C ubiquitin ligases. Curr Opin Cell Biol. 2009;21(6):816-24.

121. Sparmann A, van Lohuizen M. Polycomb silencers control cell fate, development and cancer. Nat Rev Cancer. 2006;6(11):846-56.

122. Tzivion G, Dobson M, Ramakrishnan G. FoxO transcription factors; Regulation by AKT and 14-3-3 proteins. *Biochim Biophys Acta*. 2011;1813(11):1938-45.
123. van den Heuvel S, Dyson NJ. Conserved functions of the pRB and E2F families. *Nat Rev Mol Cell Biol*. 2008;9(9):713-24.
124. Yang JY, Hung MC. A new fork for clinical application: targeting forkhead transcription factors in cancer. *Clin Cancer Res*. 2009;15(3):752-7.
125. Tan JK, Tan EL, Gan SY. Elucidating the roles of miR-372 in cell proliferation and apoptosis of nasopharyngeal carcinoma TW01 cells. *Exp Oncol*. 2014;36(3):170-3.
126. Tian RQ, Wang XH, Hou LJ, Jia WH, Yang Q, Li YX, et al. MicroRNA-372 is down-regulated and targets cyclin-dependent kinase 2 (CDK2) and cyclin A1 in human cervical cancer, which may contribute to tumorigenesis. *J Biol Chem*. 2011;286(29):25556-63.
127. Farzaneh Z, Vosough M, Agarwal T, Farzaneh M. Critical signaling pathways governing hepatocellular carcinoma behavior; small molecule-based approaches. *Cancer Cell Int*. 2021;21(1):208.
128. Wang X, Chen Y, Dong K, Ma Y, Jin Q, Yin S, et al. Effects of FER1L4-miR-106a-5p/miR-372-5p-E2F1 regulatory axis on drug resistance in liver cancer chemotherapy. *Mol Ther Nucleic Acids*. 2021;24:449-61.
129. Jiang Y, Yim SH, Xu HD, Jung SH, Yang SY, Hu HJ, et al. A potential oncogenic role of the commonly observed E2F5 overexpression in hepatocellular carcinoma. *World J Gastroenterol*. 2011;17(4):470-7.
130. Tsuji T, Miyazaki M, Fushimi K, Mihara K, Inoue Y, Ohashi R, et al. Cyclin E overexpression responsible for growth of human hepatic tumors with p21WAF1/CIP1/SDI1. *Biochem Biophys Res Commun*. 1998;242(2):317-21.
131. Koussounadis A, Langdon SP, Um IH, Harrison DJ, Smith VA. Relationship between differentially expressed mRNA and mRNA-protein correlations in a xenograft model system. *Sci Rep*. 2015;5:10775.
132. Liu H, Luo M, Wen JK. mRNA stability in the nucleus. *J Zhejiang Univ Sci B*. 2014;15(5):444-54.

Appendixes

Non-reducing buffer (RIPA), 50 ml

(10 mM Tris-HCl pH7.6, 100 mM NaCl, 1mM EDTA, 0.1% NP-40)

Tris-base (M.W. = 121.14)	60.5 mg
NaCl (M.W. = 58.44)	292.2 mg
EDTA (M.W. = 372.24)	18.6 mg
NP-40	50 μ l
Deionized water	to 50 ml

4X Reducing buffer (Laemmli's), 40 ml

(0.2 M Tris-HCl pH 6.8, 20% ME, 8% SDS, 40% glycerol)

0.5 M Tris-HCl pH 6.8	16 ml
β -mercaptoethanol	8 ml
Glycerol	16 ml
SDS (M.W. = 288.37)	3.2 g

1X TBS, 1 L

(20 mM Tris-HCl pH 7.5, 500 mM NaCl)

Tris-base (M.W. = 121.14)	2.42 g
NaCl (M.W. = 58.44)	29.24 g
Deionized water	to 1 L

5X Tris-Borate buffer (TBE), 1 L

Tris-base (M.W. = 121.14)	54 g
Boric acid (M.W. = 61.83)	27.5 g
EDTA (M.W. = 372.24)	4.16 g
Deionized water	to 1 L

1% agarose gel electrophoresis

Agarose	1 g
1X TBE	100 ml
Red safe	5 μ l

1.5 M Tris-HCl pH 8.8, 150 ml

Tris-base (M.W. = 121.14)	27.23 g
HCl	to pH 8.8
Deionized water	to 150 ml

0.5 M Tris-HCl pH 6.8, 100 ml

Tris-base (M.W. = 121.14)	6 g
HCl	to pH 6.8
Deionized water	to 100 ml

10X running buffer, 1 L

(0.25 M Tris, 1.92 M Glycine, 1% SDS)

Tris-base (M.W. = 121.14)	30.3 g
Glycine (M.W. = 75.07)	144 g
SDS (M.W. = 288.37)	10 g
Deionized water	to 1 L

10% APS (w/v)

Ammonium persulfate (M.W. = 228.2)	1,000 mg
Deionized water	10 ml

10% SDS (w/v)

SDS (M.W. = 288.37)	1 g
Deionized water	10 ml

12% resolving gel solution, 1 gel

Deionized water	2.8 ml
40% Acrylamide/Bis	1.5 ml
1.5 M Tris-HCl pH 8.8	628 μ l
10% SDS	50 μ l
10% APS	37.3 μ l
TEMED	2.67 μ l

3.75% stacking gel solution

Deionized water	1 ml
40% Acrylamide/Bis	154 μ l
0.5 M Tris-HCl pH 6.8	400 μ l
10% SDS	16 μ l
10% APS	20 μ l
TEMED	2 μ l



Table S1 Concentration of protein and preparation of protein dilution for western blot

Sample	Concentration ($\mu\text{g}/\mu\text{l}$)	100 μl protein dilution (20 $\mu\text{g}/\mu\text{l}$)	
		Volume of protein (μl)	Volume of Laemmli (μl)
HepG2 control	58.90795	33.95	66.05
HepG2 372	62.31333	32.10	67.90
JHH4 control	65.10386	30.72	69.28
JHH4 372	56.59040	35.34	64.66



VITA

NAME Pannathon Thamjamrassri

DATE OF BIRTH 03 November 1999

PLACE OF BIRTH Anan Phatthana 2 Hospital, Thoet Phra Kiat Road, Wat Chalo Subdistrict, Bang Kruai Town Municipality, Bang Kruai District, Nonthaburi Province, 11130, Thailand

INSTITUTIONS ATTENDED Kasintorn Vittaya School
Assumption College Thonburi
Mahidol University
Chulalongkorn University

HOME ADDRESS 88/303, Kratumlom 27 Road, Kratumlom Subdistrict, Samphan District, Nakhon Pathom Province, 73220, Thailand



จุฬาลงกรณ์มหาวิทยาลัย
CHULALONGKORN UNIVERSITY